A

Mathematical Appendix

The mathematics presented in this appendix is intended to supplement the discussion and formulas given in the main body of the text. The reader is assumed to be familiar with elementary calculus and complex variables, although a brief discussion of complex variables is given when appropriate. The goal of this appendix is to avoid any confusion in understanding the mathematics presented in the main text, and as such derivations and discussions are drawn out in significant detail. In particular, the techniques introduced are necessary for taking the material presented in the text one step further and experimenting with one's own mathematical models for thin film morphology. Mathematical rigor is not stressed in this discussion; for a more complete derivation and discussion of the following topics, see [26, 45, 102].

A.1 Special Functions

In the mathematical description of thin film morphology, a number of special functions are used that may be unfamiliar to the reader, and it is useful to describe their behavior and properties. In particular, a class of functions called Bessel functions are significantly utilized. We begin with the Bessel function of the first kind.

A.1.1 Bessel Function of the First Kind

The nth order Bessel function of the first kind, denoted $J_n(x)$, is defined as

$$J_n(x) = \sum_{j=0}^{\infty} \frac{(-1)^j}{j!\Gamma(n+j+1)} \left(\frac{x}{2}\right)^{2j+n}, \tag{A.1}$$

where $\Gamma(x)$ is the gamma function discussed in Sect. A.1.4. In particular, for $n = 0$,

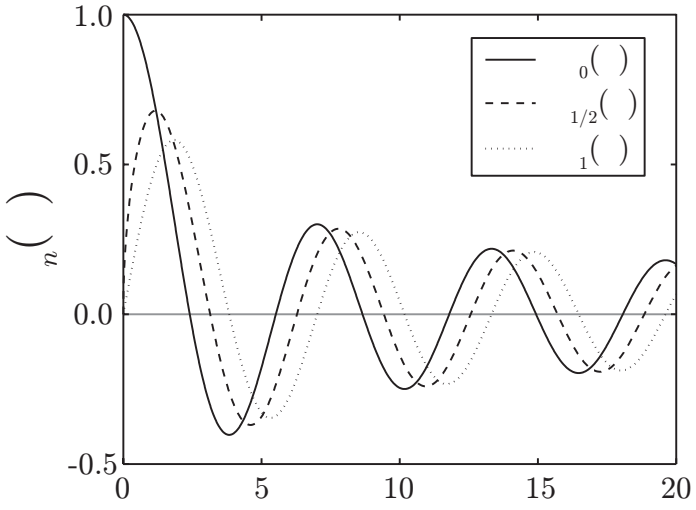

Fig. A.1. Ordinary Bessel functions $J_n(x)$ of order $n = 0$, $1/2$, and 1.

$$J_0(x) = \sum_{j=0}^{\infty} \frac{(-1)^j}{(j!)^2} \left(\frac{x}{2}\right)^{2j}. \tag{A.2}$$

Bessel functions have a characteristic oscillatory behavior, and for asymptotically large x behave as cos functions,

$$J_n(x) \sim \sqrt{\frac{2}{\pi x}} \cos\left(x - \frac{n\pi}{2} - \frac{\pi}{4}\right), \quad x \gg \left|n^2 - \frac{1}{4}\right|. \tag{A.3}$$

This oscillatory behavior is clear from Fig. A.1. Similarly for small x, from the power series in (A.1),

$$J_n(x) \sim \frac{1}{n!} \left(\frac{x}{2}\right)^n, \quad x \ll \sqrt{n+1}. \tag{A.4}$$

An important relation involving Bessel functions is the orthogonality relation on a semi-infinite interval,

$$\int_0^{\infty} x J_n(ax) J_n(bx) \mathrm{d}x = \frac{1}{a} \delta(a-b), \tag{A.5}$$

where $\delta(x)$ is the delta function, described in Sect. A.1.5, which implies that the integral is zero unless $a = b$. This property of Bessel functions is a key reason why they are incorporated into models for 2+1 dimensional surfaces

because this orthogonality leads to analytical expressions for surface statistics such as the power spectral density function.

Another formula that is used frequently is the relation

$$\int_0^{2\pi} \mathrm{e}^{\mathrm{i}x\cos\theta}\mathrm{d}\theta = 2\pi J_0(x). \tag{A.6}$$

This can be derived by expanding the exponential in a power series,

$$\int_0^{2\pi} \sum_{n=0}^{\infty} \frac{(\mathrm{i}x\cos\theta)^n}{n!}\mathrm{d}\theta = \sum_{n=0}^{\infty} \frac{(\mathrm{i}x)^n}{n!} \int_0^{2\pi} \cos^n\theta\mathrm{d}\theta. \tag{A.7}$$

Using complex variable techniques as outlined in Sect. A.2, it can be shown that

$$\int_0^{2\pi} \cos^n\theta\mathrm{d}\theta = \begin{cases} 0, & n \text{ odd}, \\ \frac{2\pi}{2^n}\frac{n!}{[(n/2)!]^2}, & n \text{ even}. \end{cases} \tag{A.8}$$

This result gives, with $n = 2j$,

$$\begin{aligned} \sum_{n=0}^{\infty} \frac{(\mathrm{i}x)^n}{n!} \int_0^{2\pi} \cos^n\theta\mathrm{d}\theta &= \sum_{j=0}^{\infty} \frac{(\mathrm{i}x)^{2j}}{(2j)!}\frac{2\pi}{2^{2j}}\frac{(2j)!}{(j!)^2} \\ &= 2\pi\sum_{j=0}^{\infty}\frac{(-1)^j}{(j!)^2}\left(\frac{x}{2}\right)^{2j} \\ &= 2\pi J_0(x), \end{aligned}$$

using the definition of $J_0(x)$ from (A.2).

A.1.2 Modified Bessel Function of the First Kind

The modified Bessel function of the first kind, denoted by $I_n(x)$, is a notation used to denote the ordinary Bessel function of the first kind for a purely complex argument. The modified class of functions is defined as

$$I_n(x) = \mathrm{i}^{-n}J_n(\mathrm{i}x). \tag{A.9}$$

These functions have an exponential behavior for large x,

$$I_n(x) \sim \frac{\mathrm{e}^x}{\sqrt{2\pi x}}, \quad x \gg \left|n^2 - \frac{1}{4}\right|. \tag{A.10}$$

The most useful relation for our purposes involving the modified Bessel function of the first kind is obtained from (A.6) with the substitution $t = \mathrm{i}x$,

$$\int_0^{2\pi} \mathrm{e}^{t\cos\theta}\mathrm{d}\theta = 2\pi I_0(t). \tag{A.11}$$

A.1.3 Modified Bessel Function of the Second Kind

The modified Bessel function of the second kind, denoted $K_n(x)$, is defined as

$$K_n(x) = \frac{\pi}{2}\frac{I_{-n}(x) - I_n(x)}{\sin n\pi}. \tag{A.12}$$

This expression is indeterminate for integer n, and an appropriate limit must be taken for integer n. The limiting behavior of this function is, for large x,

$$K_n(x) \sim \sqrt{\frac{\pi}{2x}}\mathrm{e}^{-x}, \quad x \gg \left|n^2 - \frac{1}{4}\right|, \tag{A.13}$$

and for small x and $|n| < 1$, using (A.1),

$$K_n(x) \sim \frac{\Gamma(n)}{2}\left(\frac{2}{x}\right)^n - \frac{\Gamma(1-n)}{2n}\left(\frac{x}{2}\right)^n, \quad x \ll \sqrt{n+1}, \tag{A.14}$$

where $\Gamma(x)$ is the gamma function described in Sect. A.1.4. Two specific cases are of interest, the behavior of the function for orders 0 and 1/2, given by [4, 15]:

$$K_{1/2}(x) = \sqrt{\frac{\pi}{2x}}\mathrm{e}^{-x}, \tag{A.15}$$

$$K_0(x) \sim -\ln x. \tag{A.16}$$

A.1.4 Gamma Function

The gamma function $\Gamma(x)$ is defined as

$$\Gamma(x) = \int_0^\infty s^{x-1}\mathrm{e}^{-s}\mathrm{d}s. \tag{A.17}$$

This function is most commonly known for providing a continuous generalization of the factorial function $x! = x(x-1)(x-2)\cdots 2\cdot 1$, as can be shown by an integration by parts,

$$\begin{aligned}
\Gamma(x) &= \int_0^\infty s^{x-1}\mathrm{e}^{-s}\mathrm{d}s \\
&= \left[-s^{x-1}\mathrm{e}^{-s}\right]_0^\infty + \int_0^\infty (x-1)s^{x-2}\mathrm{e}^{-s}\mathrm{d}s \\
&= (x-1)\int_0^\infty s^{x-2}\mathrm{e}^{-s}\mathrm{d}s \\
&= (x-1)\Gamma(x-1).
\end{aligned}$$

Using this property of $\Gamma(x)$, coupled with the value of $\Gamma(1) = 1$, it follows by induction that if x is an integer, then

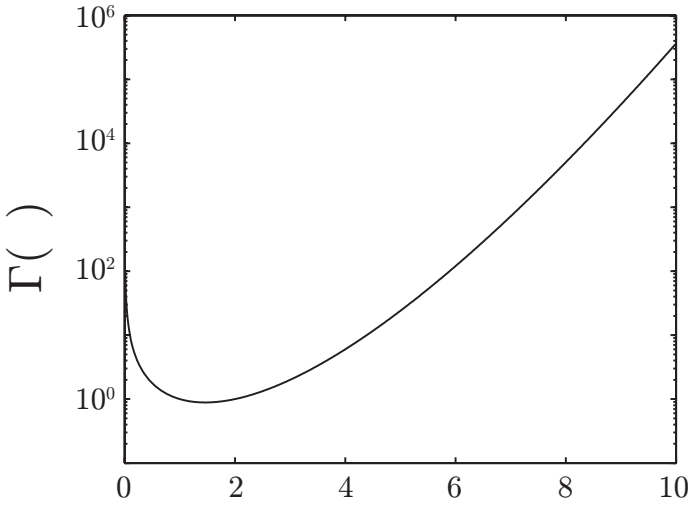

Fig. A.2. Gamma function $\Gamma(x)$ for $0 < x \leq 10$. For integer x, $\Gamma(x) = (x-1)!$.

$$\Gamma(x) = (x-1)!. \tag{A.18}$$

However, whereas the factorial function is only defined for positive integers, $\Gamma(x)$ is continuously defined for $x > 0$. A graph of $\Gamma(x)$ is provided in Fig. A.2. Another useful property of $\Gamma(x)$ is

$$\Gamma(x)\Gamma(1-x) = \frac{\pi}{\sin x\pi}, \tag{A.19}$$

which was used to find the series expansion of the modified Bessel function of the second kind in the previous section.

A.1.5 Delta Function

The delta function $\delta(x)$ can be thought of conceptually as an infinitely short pulse. For most physical purposes, the delta function can be defined as

$$\delta(x) = \begin{cases} \infty, & x = 0, \\ 0, & x \neq 0, \end{cases} \tag{A.20}$$

with the additional property that

$$\int_{-\infty}^{\infty} \delta(x)\mathrm{d}x = 1. \tag{A.21}$$

However, the traditional Riemann integral of any well-behaved function that is zero everywhere except at one point is zero, which contradicts (A.21). This contradiction arises because $\delta(x)$ is not a true function, and a rigorous mathematical definition of the delta function would be beyond the scope of this discussion. Even though $\delta(x)$ is not a function itself, it can be thought of as the limit of a sequence of functions whose properties approach the properties of the delta function. For example, consider the function of x defined by the limit

$$f(x) = \lim_{\eta \to 0^+} \frac{1}{\pi} \frac{\eta}{x^2 + \eta^2}, \tag{A.22}$$

where $\lim_{\eta \to 0^+}$ means that the limit is approaching zero from positive η. This can be thought of as a sequence of functions of x that possesses all the properties of a delta function. For example, the integral of each member of the sequence is given by

$$\begin{aligned} \int_{-\infty}^{\infty} \frac{1}{\pi} \frac{\eta}{x^2 + \eta^2} \mathrm{d}x &= \frac{1}{\pi} \left[\tan^{-1} \frac{x}{\eta} \right]_{-\infty}^{\infty} \\ &= \frac{1}{\pi} \left[\frac{\pi}{2} + \frac{\pi}{2} \right] \\ &= 1, \end{aligned}$$

which is independent of η. Also, for $x \neq 0$,

$$\lim_{\eta \to 0^+} \frac{1}{\pi} \frac{\eta}{x^2 + \eta^2} = 0, \tag{A.23}$$

and, for $x = 0$,

$$\lim_{\eta \to 0^+} \frac{1}{\pi} \frac{\eta}{0^2 + \eta^2} = \lim_{\eta \to 0^+} \frac{1}{\pi \eta} = \infty. \tag{A.24}$$

Thus, if we make the designation

$$\delta(x) = \lim_{\eta \to 0^+} \frac{1}{\pi} \frac{\eta}{x^2 + \eta^2}, \tag{A.25}$$

the properties in (A.20) and (A.21) are satisfied. There are many such ways to define the delta function as the limit of a series of functions. The most useful definition for our purposes is the relation

$$\delta(x) = \frac{1}{2\pi} \int_{-\infty}^{\infty} \mathrm{e}^{\mathrm{i}kx} \mathrm{d}k, \tag{A.26}$$

or, more specifically, the limit of the following sequence with integer n,

$$\delta(x) = \lim_{n \to \infty} \frac{1}{2\pi} \int_{-n\pi/x}^{n\pi/x} \mathrm{e}^{\mathrm{i}kx} \mathrm{d}k. \tag{A.27}$$

Let us verify that this is indeed a valid definition of the delta function. We can perform the integration with $x \neq 0$ to obtain

$$\begin{aligned}\int_{-n\pi/x}^{n\pi/x} \mathrm{e}^{\mathrm{i}kx}\mathrm{d}k &= \left[\frac{1}{\mathrm{i}x}\mathrm{e}^{\mathrm{i}kx}\right]_{-n\pi/x}^{n\pi/x} \\ &= \left[\frac{1}{\mathrm{i}x}\left(\mathrm{e}^{\mathrm{i}n\pi} - \mathrm{e}^{-\mathrm{i}n\pi}\right)\right] \\ &= \frac{2\sin n\pi}{x}.\end{aligned}$$

In (A.27), n is an integer, so the value of this integral is zero for each n when $x \neq 0$. Clearly, when $x = 0$, the integral in (A.27) becomes

$$\int_{-\infty}^{\infty} \mathrm{e}^{0}\mathrm{d}k = \infty. \tag{A.28}$$

Thus, the limit in (A.27) satisfies the properties of (A.20). Now we must show that (A.21) holds as well. To do so, consider the general case of the limits of integration in (A.27) to be any number a, and examine the limit as $a \to \infty$.

$$\lim_{a\to\infty} \frac{1}{2\pi}\int_{-\infty}^{\infty}\int_{-a}^{a} \mathrm{e}^{\mathrm{i}kx}\mathrm{d}k\mathrm{d}x = \lim_{a\to\infty} \frac{1}{2\pi}\int_{-\infty}^{\infty} \frac{2\sin ax}{x}\mathrm{d}x. \tag{A.29}$$

The variable a was used instead of $n\pi/x$ because the special case of $n\pi/x$ leads to a question of convergence of the integral; in the end the result will not depend on a and will be valid for any a. This is the price that is paid for avoiding a mathematically rigorous derivation because interchanging the orders of integration is not necessarily justified, but the results we obtain will be correct. If we change variables in (A.29) to $t = ax$, the integral then becomes

$$\lim_{a\to\infty} \frac{1}{2\pi}\int_{-\infty}^{\infty} \frac{2\sin ax}{x}\mathrm{d}x = \lim_{a\to\infty} \frac{1}{\pi}\int_{-\infty}^{\infty} \frac{\sin t}{t}\mathrm{d}t, \tag{A.30}$$

which is independent of a. Using complex variable techniques, the value of the last integral can be shown to be

$$\int_{-\infty}^{\infty} \frac{\sin t}{t}\mathrm{d}t = \pi, \tag{A.31}$$

so the integral of each member of the sequence in (A.27) is one, and (A.21) is satisfied.

The utility of the delta function lies in what is commonly called a "sifting" property,

$$\int_{-\infty}^{\infty} f(x)\delta(x)\mathrm{d}x = f(0) \tag{A.32}$$

for a well-behaved function $f(x)$ or, more generally,

$$\int_{-\infty}^{\infty} f(x)\delta(x-a)\mathrm{d}x = f(a). \tag{A.33}$$

Because $\delta(x-a)=0$ for $x \neq a$, the only point in the domain of integration that matters is $x=a$. In addition, the delta function is normalized to one from (A.21), therefore the result of the integral is simply the function value at $x=a$. Thus, when the delta function appears under an integral, it "picks out" the value of the function it multiplies and renders the integral trivial to evaluate.

The previous derivations have been carried out in one dimension, but the delta function can be defined in multiple dimensions. For example, the two-dimensional delta function can be written as

$$\delta^2(\mathbf{x}) = \delta(x)\delta(y), \tag{A.34}$$

where $\mathbf{x}=(x,y)$ and the symbol δ^2 is used to denote that the delta function is two-dimensional; it does not mean that the delta function is squared. In general,

$$\delta^d(\mathbf{x}) = \prod_{j=1}^{d} \delta(x_d), \tag{A.35}$$

where $\mathbf{x}$ is a d-dimensional vector, and x_d are Cartesian coordinates. It should also be noted that these definitions only hold in Cartesian coordinates, for example, in two-dimensional polar coordinates [16],

$$\delta^2(\mathbf{x}) = \frac{\delta(r)}{\pi|r|}. \tag{A.36}$$

A.2 Complex Integrals

For the derivations that are included in the following sections, certain concepts in complex variables are required to carry out the mathematics. For readers unfamiliar with complex numbers, we present a short discussion of the concepts needed to follow the mathematics that ensues.

Complex numbers can be represented in terms of real numbers along with the symbol i, which is defined as $\mathrm{i}^2=-1$. A complex number z can be written in terms of the real numbers x and y as

$$z = x + \mathrm{i}y. \tag{A.37}$$

Carrying out operations with complex numbers follows the same rules as those with real numbers, assuming that whenever i^2 appears, it is replaced with -1. One of the most well-known formulas in complex numbers is Euler's formula,

$$\mathrm{e}^{\mathrm{i}x} = \cos x + \mathrm{i}\sin x, \tag{A.38}$$

which can be shown by expanding the exponential in a Taylor series,

$$\begin{aligned}
\mathrm{e}^{\mathrm{i}x} &= \sum_{n=0}^{\infty} \frac{(\mathrm{i}x)^n}{n!} \\
&= \sum_{j=0}^{\infty} \frac{(\mathrm{i}x)^{2j}}{(2j)!} + \sum_{j=0}^{\infty} \frac{(\mathrm{i}x)^{2j+1}}{(2j+1)!} \\
&= \sum_{j=0}^{\infty} \frac{(-1)^j x^{2j}}{(2j)!} + \mathrm{i} \sum_{j=0}^{\infty} \frac{(-1)^j x^{2j+1}}{(2j+1)!} \\
&= \cos x + \mathrm{i} \sin x.
\end{aligned}$$

Integration of a function of a complex variable is defined in a similar manner to integration in real variables, except for the specification of a path in complex variables. In ordinary single-variable calculus, the integral is taken along the x-axis, but in complex variables, an integral can be taken along any path in the x–y plane. Integration of a complex function is of interest here because it allows for the evaluation of real-valued integrals that are difficult to evaluate without complex numbers. We are interested in the specific case of an integral over a closed path, or contour, in the complex plane. If the function $f(z)$ has no singularities inside a contour C and is a function of z only and not its complex conjugate, then

$$\oint_C f(z)\mathrm{d}z = 0. \tag{A.39}$$

Such a function is called an analytic function in the domain enclosed by C. If $f(z)$ has a singularity at $z = z_0$ of the form

$$f(z) = \frac{g(z)}{(z - z_0)^{n+1}}, \tag{A.40}$$

where $g(z)$ is a well-behaved function with no singularities in the contour, then

$$\oint_C f(z)\mathrm{d}z = \frac{2\pi\mathrm{i}}{n!} \lim_{z \to z_0} \frac{\mathrm{d}^n}{\mathrm{d}z^n} g(z). \tag{A.41}$$

This is known as Cauchy's residue theorem, and its proof is beyond the scope of our discussion. The residue of $f(z)$ is defined as

$$\mathrm{Res} f(z_0) = \frac{1}{n!} \lim_{z \to z_0} \frac{\mathrm{d}^n}{\mathrm{d}z^n} g(z). \tag{A.42}$$

The utility of this result lies in expressing the contour integral in terms of a real-valued integral. As an example, we derive a result used to prove (A.8). Consider the contour integral over a semicircular contour of radius R in the upper half-plane of the integrand $(1 + z^2)^{-(n+1)}$,

$$\oint \frac{\mathrm{d}z}{(1+z^2)^{n+1}} = \int_{-R}^{R} \frac{\mathrm{d}x}{(1+x^2)^{n+1}} + \int_{C_S} \frac{\mathrm{d}z}{(1+z^2)^{n+1}}.$$

The integral over the semicircle $\left(z = R\mathrm{e}^{\mathrm{i}\theta}\right)$ behaves as

$$\int_{C_S} \frac{\mathrm{d}z}{(1+z^2)^{n+1}} = \int_0^{\pi} \frac{\mathrm{i}R\mathrm{e}^{\mathrm{i}\theta}\mathrm{d}\theta}{(1+R^2\mathrm{e}^{2\mathrm{i}\theta})^{n+1}} \sim O(R^{-2n-1}),$$

and approaches zero for $n \geq 1$ as $R \to \infty$. The contour integral has one singularity in the domain of integration at $z = \mathrm{i}$ of order $n+1$. The residue at this point is given by

$$\begin{aligned}
\mathrm{Res} f(\mathrm{i}) &= \lim_{z\to\mathrm{i}} \frac{1}{n!}\frac{\mathrm{d}^n}{\mathrm{d}z^n}\left[\frac{1}{(z+\mathrm{i})^{n+1}}\right] \\
&= \lim_{z\to\mathrm{i}} \frac{1}{n!}\left[\frac{(n+1)(n+2)\cdots(2n)(-1)^n}{(z+\mathrm{i})^{2n+1}}\right] \\
&= \frac{1}{n!}\left[\frac{(n+1)(n+2)\cdots(2n)(\mathrm{i}^2)^n}{2^{2n+1}\mathrm{i}^{2n+1}}\right] \\
&= \frac{1}{n!}\left[\frac{(2n)!}{n!}\frac{1}{2^{2n+1}\mathrm{i}}\right] \\
&= \frac{1}{2^{2n+1}\mathrm{i}}\frac{(2n)!}{(n!)^2}.
\end{aligned}$$

By Cauchy's theorem,

$$\oint \frac{\mathrm{d}z}{(1+z^2)^{n+1}} = 2\pi\mathrm{i}\left[\frac{1}{2^{2n+1}\mathrm{i}}\frac{(2n)!}{(n!)^2}\right] = \frac{\pi}{2^{2n}}\frac{(2n)!}{(n!)^2}.$$

It follows that

$$\int_{-\infty}^{\infty} \frac{\mathrm{d}x}{(1+x^2)^{n+1}} = \frac{\pi}{2^{2n}}\frac{(2n)!}{(n!)^2}.$$

Now, make the transformation $x = \tan\theta$, $\mathrm{d}x = \sec^2\theta\mathrm{d}\theta$,

$$\begin{aligned}
\int_{-\infty}^{\infty} \frac{\mathrm{d}x}{(1+x^2)^{n+1}} &= \int_{-\pi/2}^{\pi/2} \frac{\sec^2\theta\mathrm{d}\theta}{(1+\tan^2\theta)^{n+1}} \\
&= \int_{-\pi/2}^{\pi/2} \frac{\sec^2\theta\mathrm{d}\theta}{\sec^{2n+2}\theta} \\
&= \int_{-\pi/2}^{\pi/2} \cos^{2n}\theta\mathrm{d}\theta.
\end{aligned}$$

Because $\cos^2\theta$ is periodic in π, the integral over the interval $[-\pi/2, \pi/2]$ is an integral over one period, so shifting the domain to $[0, \pi]$ will not affect the integral because the integral is still over one full period. Extending the domain to $[0, 2\pi]$ will double the value of the integral because the domain $[0, 2\pi]$ is over two full periods, which gives

$$\int_0^{2\pi} \cos^{2n}\theta\mathrm{d}\theta = 2\int_0^{\pi} \cos^{2n}\theta\mathrm{d}\theta = \frac{2\pi}{2^{2n}}\frac{(2n)!}{(n!)^2}. \tag{A.43}$$

This complex variable contour integration technique is very powerful, and can be used to show the following two results that are utilized in this appendix,

$$\int_{-\infty}^{\infty} \frac{\sin x}{x} \mathrm{d}x = \pi$$
$$\int_0^{2\pi} \frac{\mathrm{d}\theta}{(1 - a\cos\theta)^2} = \frac{2\pi}{(1-a^2)^{3/2}}.$$

These results are left to the reader to verify.

A.3 Fourier Transform of a Product

The Fourier transform of a function is the representation of a function in frequency space. The set of functions $\left\{\mathrm{e}^{\mathrm{i}kx}\right\}$, for real k, constitutes a complete set of functions, therefore any arbitrary function $f(x)$ can be decomposed into a sum of these functions. Recall that $\mathrm{e}^{\mathrm{i}kx} = \cos kx + \mathrm{i}\sin kx$, so this statement suggests that $f(x)$ can be represented by a weighted sum of waves of different wavenumbers k. If $f(x)$ is not periodic, an integral over all real k will be required to represent $f(x)$ in frequency space. However, if $f(x)$ is periodic, only the harmonic frequencies corresponding to the period of $f(x)$ will contribute, which is called a Fourier series because the sum is discrete as opposed to an integral. This discussion suggests that any function $f(x)$ can be represented as

$$f(x) = \int_{-\infty}^{\infty} \hat{f}(k)\mathrm{e}^{-\mathrm{i}kx}\mathrm{d}k, \tag{A.44}$$

where $\hat{f}(k)$ is the Fourier transform of $f(x)$. The integral is simply a sum over all frequencies, or wavenumbers k, with an appropriate weight for each wavenumber, given by $\hat{f}(k)$. In this section, unless otherwise noted, all integrals are taken from $-\infty$ to ∞. Multiplying both sides of this equation by $\mathrm{e}^{\mathrm{i}k'x}$ and integrating over x gives

$$\int f(x)\mathrm{e}^{\mathrm{i}k'x}\mathrm{d}x = \int\int \hat{f}(k)\mathrm{e}^{\mathrm{i}(k'-k)x}\mathrm{d}k\mathrm{d}x. \tag{A.45}$$

However, (A.26) can be used to perform the integral over x as a delta function,

$$\int f(x)\mathrm{e}^{\mathrm{i}k'x}\mathrm{d}x = 2\pi\int \hat{f}(k)\delta(k'-k)\mathrm{d}k$$
$$\frac{1}{2\pi}\int f(x)\mathrm{e}^{\mathrm{i}k'x}\mathrm{d}x = \hat{f}(k').$$

Therefore, we can define the Fourier transform of $f(x)$, denoted by $\hat{f}(k)$ or $\mathcal{F}\{f(x)\}$, as

$$\mathcal{F}\{f(x)\} = \hat{f}(k) = \frac{1}{2\pi}\int f(x)\mathrm{e}^{\mathrm{i}kx}\mathrm{d}x. \tag{A.46}$$

Motivated by this definition in one dimension, in d-dimensions the Fourier transform becomes

$$\mathcal{F}\{f(\mathbf{x})\} = \frac{1}{(2\pi)^d}\int f(\mathbf{x})\mathrm{e}^{\mathrm{i}\mathbf{k}\cdot\mathbf{x}}\mathrm{d}\mathbf{x}. \tag{A.47}$$

Now, consider the Fourier transform of the product of two functions $f(x)g(x)$. This can be written as, using (A.26),

$$\begin{aligned}\mathcal{F}\{f(x)g(x)\} &= \frac{1}{2\pi}\int f(x)g(x)\mathrm{e}^{\mathrm{i}kx}\mathrm{d}x \\ &= \frac{1}{2\pi}\int\int f(x)g(x')\delta(x'-x)\mathrm{e}^{\mathrm{i}kx}\mathrm{d}x\mathrm{d}x' \\ &= \frac{1}{(2\pi)^2}\int\int\int f(x)g(x')\mathrm{e}^{\mathrm{i}k'(x'-x)}\mathrm{e}^{\mathrm{i}kx}\mathrm{d}x\mathrm{d}x'\mathrm{d}k' \\ &= \int \mathrm{d}k'\left(\frac{1}{2\pi}\int \mathrm{d}x f(x)\mathrm{e}^{\mathrm{i}(k-k')x}\right)\left(\frac{1}{2\pi}\int \mathrm{d}x' g(x')\mathrm{e}^{\mathrm{i}k'x'}\right).\end{aligned}$$

Let us define the convolution $(F{*}G)(k)$ of two functions $F(k)$ and $G(k)$ as

$$(F{*}G)(k) = \int \mathrm{d}k' F(k-k')G(k'). \tag{A.48}$$

It then follows that

$$\mathcal{F}\{f(x)g(x)\} = \mathcal{F}\{f(x)\} * \mathcal{F}\{g(x)\}; \tag{A.49}$$

that is, the Fourier transform of the product of two functions is the convolution of the individual Fourier transforms. Note that the convolution was defined in terms of Cartesian coordinates, and in higher dimensions, Cartesian coordinates must be used to express the convolution.

A specific case of a Fourier transform that is useful is the two-dimensional Fourier transform of a product of two functions of r in polar coordinates. The Fourier transform of the product will simply be the convolution of the individual Fourier transforms, but the form can be simplified further because both functions are only functions of r.

$$\begin{aligned}\mathcal{F}\{f(r)g(r)\} &= \mathcal{F}\{f(r)\} * \mathcal{F}\{g(r)\} \\ &= \left(\frac{1}{(2\pi)^2}\int_0^{2\pi}\int_0^{\infty} f(r)\mathrm{e}^{\mathrm{i}kr\cos\theta} r\mathrm{d}r\mathrm{d}\theta\right) \\ &\quad * \left(\frac{1}{(2\pi)^2}\int_0^{2\pi}\int_0^{\infty} g(r)\mathrm{e}^{\mathrm{i}kr\cos\theta} r\mathrm{d}r\mathrm{d}\theta\right).\end{aligned}$$

Using (A.6), the integration over θ can be carried out because the functions f and g do not depend on θ,

$$\mathcal{F}\{f(r)g(r)\} = \left(\frac{1}{2\pi}\int_0^\infty f(r)J_0(kr)r\mathrm{d}r\right) * \left(\frac{1}{2\pi}\int_0^\infty g(r)J_0(kr)r\mathrm{d}r\right). \tag{A.50}$$

This form invites the definition of the Hankel transform $\mathcal{H}$,

$$\mathcal{H}\{f(r)\} = \int_0^\infty f(r)J_0(kr)r\mathrm{d}r, \tag{A.51}$$

and the Fourier transform of $f(r)g(r)$ can be written as

$$\mathcal{F}\{f(r)g(r)\} = \frac{1}{(2\pi)^2}\mathcal{H}\{f(r)\} * \mathcal{H}\{g(r)\}. \tag{A.52}$$

If the autocorrelation function $R(r)$ for a surface is the product of two functions, $R(r) = f(r)g(r)$, then the power spectral density function of the surface, which is equal to the interface width squared (w^2) times the Fourier transform of the autocorrelation function from (2.16), can be written as

$$P(k) = \frac{w^2}{(2\pi)^2}\mathcal{H}\{f(r)\} * \mathcal{H}\{g(r)\}. \tag{A.53}$$

This result is used extensively in the following sections. When using this formula, the convolution of two functions $F(r)$ and $G(r)$ expressed in terms of the polar coordinate $r = \sqrt{x^2 + y^2}$ must be written as

$$F(r) * G(r) = \int\int F\left(\sqrt{(x-x')^2 + (y-y')^2}\right) G\left(\sqrt{(x')^2 + (y')^2}\right) \mathrm{d}x'\mathrm{d}y', \tag{A.54}$$

where the integration is over the entire domain of x' and y'. The resulting integral can then be converted to a coordinate system where it is conveniently evaluated.

A.4 Power Spectral Density Functions

The mathematical details of finding the analytic forms of power spectral density functions given in the text are included in the following sections. The mathematics are carried out for the PSD in 2+1 dimensions, but similar steps may be taken to find the form in 1+1 dimensions. A summary of the results in 1+1 dimensions and 2+1 dimensions is given in Sect. A.4.5.

A.4.1 Self-Affine Surface – Exponential Model

The exponential model for the autocorrelation function of a self-affine surface as discussed in Sect. 3.2 is given by

$$R(r) = \exp\left[-\left(\frac{r}{\xi}\right)^{2\alpha}\right]. \tag{A.55}$$

The PSD of a surface in 2+1 dimensions is related to the Hankel transform of the autocorrelation function,

$$P(k) = \frac{w^2}{2\pi}\int_0^\infty R(r)J_0(kr)r\mathrm{d}r = \frac{w^2}{2\pi}\mathcal{H}\left\{R(r)\right\}. \tag{A.56}$$

Using (A.6), the Hankel transform of the autocorrelation function is given by

$$\mathcal{H}\left\{\exp\left[-\left(\frac{r}{\xi}\right)^{2\alpha}\right]\right\} = \frac{1}{2\pi}\int_0^{2\pi}\int_0^\infty r\exp\left[-\left(\frac{r}{\xi}\right)^{2\alpha}\right]\exp\left[\mathrm{i}kr\cos\theta\right]\mathrm{d}r\mathrm{d}\theta.$$

A Taylor expansion of the second exponential gives

$$\mathcal{H}\left\{\exp\left[-\left(\frac{r}{\xi}\right)^{2\alpha}\right]\right\} = \frac{1}{2\pi}\sum_{n=0}^\infty\int_0^{2\pi}\int_0^\infty r\exp\left[-\left(\frac{r}{\xi}\right)^{2\alpha}\right]\frac{(\mathrm{i}kr\cos\theta)^n}{n!}\mathrm{d}r\mathrm{d}\theta.$$

Rearranging the integrals gives

$$\mathcal{H}\left\{\exp\left[-\left(\frac{r}{\xi}\right)^{2\alpha}\right]\right\} = \sum_{n=0}^\infty\int_0^{2\pi}\frac{(\mathrm{i}k\cos\theta)^n}{2\pi n!}\mathrm{d}\theta\int_0^\infty r^{n+1}\exp\left[-\left(\frac{r}{\xi}\right)^{2\alpha}\right]\mathrm{d}r. \tag{A.57}$$

Carrying out the angular integration with (A.43), this expression becomes

$$\mathcal{H}\left\{\exp\left[-\left(\frac{r}{\xi}\right)^{2\alpha}\right]\right\} = \sum_{j=0}^\infty\frac{1}{(j!)^2}\left(-\frac{k^2}{4}\right)^j\int_0^\infty r^{2j+1}\exp\left[-\left(\frac{r}{\xi}\right)^{2\alpha}\right]\mathrm{d}r.$$

However, we can introduce the change of variable $s = (r/\xi)^{2\alpha}$ to write the Hankel transform as

$$\mathcal{H}\left\{\exp\left[-\left(\frac{r}{\xi}\right)^{2\alpha}\right]\right\} = \frac{\xi^2}{2\alpha}\sum_{j=0}^\infty\frac{1}{(j!)^2}\left(-\frac{k^2\xi^2}{4}\right)^j\int_0^\infty s^{(j+1)/\alpha-1}\mathrm{e}^{-s}\mathrm{d}s.$$

The integral can be written in terms of the gamma function as

$$\mathcal{H}\left\{\exp\left[-\left(\frac{r}{\xi}\right)^{2\alpha}\right]\right\} = \frac{\xi^2}{2\alpha}\sum_{j=0}^\infty\frac{\Gamma\left(\frac{j+1}{\alpha}\right)}{(j!)^2}\left(-\frac{k^2\xi^2}{4}\right)^j, \tag{A.58}$$

which leads to the PSD

$$P(k) = \frac{w^2\xi^2}{4\pi\alpha}\sum_{j=0}^\infty\frac{\Gamma\left(\frac{j+1}{\alpha}\right)}{(j!)^2}\left(-\frac{k^2\xi^2}{4}\right)^j. \tag{A.59}$$

For $\alpha = 1$, the sum can be explicitly computed, and the exponential model predicts the self-affine PSD in 2+1 dimensions to be

$$P(k) = \frac{w^2\xi^2}{4\pi}\exp\left[-\frac{k^2\xi^2}{4}\right]. \tag{A.60}$$

However, this form does not behave well as $\alpha \to 0$, and we investigate the K-correlation model in the next section that better deals with this behavior.

A.4.2 Self-Affine Surface – *K*-Correlation Model

The form of the autocorrelation function proposed by Palasantzas [118] for a self-affine surface is

$$R(r) = \frac{1}{a\Gamma(\alpha+1)} \left(\frac{r}{2\xi\sqrt{a}}\right)^{\alpha} K_{\alpha}\left(\frac{r}{\xi\sqrt{a}}\right), \tag{A.61}$$

where $K_{\alpha}(x)$ is the α-ordered modified Bessel function of the second kind introduced in Sect. A.1.3, and a is defined implicitly by

$$a = \frac{1}{2\alpha}\left[1 - \frac{1}{(1+ak_c^2\xi^2)^{\alpha}}\right], \tag{A.62}$$

where k_c is the upper cutoff frequency of the self-affine behavior for the surface, which would be inversely proportional to the lattice size. If we consider the continuum limit of no upper frequency cutoff, $k_c \to \infty$, we find that $a = (2\alpha)^{-1}$ for $\alpha \neq 0$, which gives

$$R(r) = \frac{\alpha}{2^{\alpha-1}\Gamma(\alpha+1)} \left(\frac{r}{\xi}\sqrt{2\alpha}\right)^{\alpha} K_{\alpha}\left(\frac{r}{\xi}\sqrt{2\alpha}\right). \tag{A.63}$$

The case where $\alpha = 0$ is obtained by taking the appropriate limit of the above expressions as $\alpha \to 0$, which gives

$$R(r) = \frac{1}{\tilde{a}} K_0\left(\frac{r}{\xi\sqrt{\tilde{a}}}\right) \quad \text{for } \alpha = 0, \tag{A.64}$$

where $\tilde{a}$ satisfies

$$\tilde{a} = \frac{1}{2}\ln\left(1+\tilde{a}k_c^2\xi^2\right). \tag{A.65}$$

Note that when $\alpha = 0$, taking the limit as $k_c \to \infty$ leads to a divergence, and the discrete nature of the surface profile must be taken into account by considering k_c when $\alpha = 0$. We are concerned only with the continuum limit of the autocorrelation function, and thus restrict the discussion to the interval $0 < \alpha \leq 1$. However, it is important to note that this model behaves correctly in the limit as $\alpha \to 0$ because $K_0(x) \sim -\ln x$ for small x, as opposed to the exponential correlation model which does not.

To find the PSD for $0 < \alpha \leq 1$, we need to find the Hankel transform of the autocorrelation function given in (A.63), which requires the evaluation of the integral

$$I = \int_0^{\infty} r^{\alpha+1} K_{\alpha}\left(\frac{r}{\xi}\sqrt{2\alpha}\right) J_0(kr)\mathrm{d}r. \tag{A.66}$$

To accomplish this, expand the Bessel function as (A.2),

$$\begin{aligned} I &= \int_0^{\infty} r^{\alpha+1} K_{\alpha}\left(\frac{r}{\xi}\sqrt{2\alpha}\right) \sum_{j=0}^{\infty} \frac{(-1)^j}{(j!)^2}\left(\frac{kr}{2}\right)^{2j} \mathrm{d}r \\ &= \sum_{j=0}^{\infty} \frac{(-1)^j}{(j!)^2}\left(\frac{k}{2}\right)^{2j} \int_0^{\infty} r^{\alpha+1+2j} K_{\alpha}\left(\frac{r}{\xi}\sqrt{2\alpha}\right) \mathrm{d}r. \end{aligned}$$

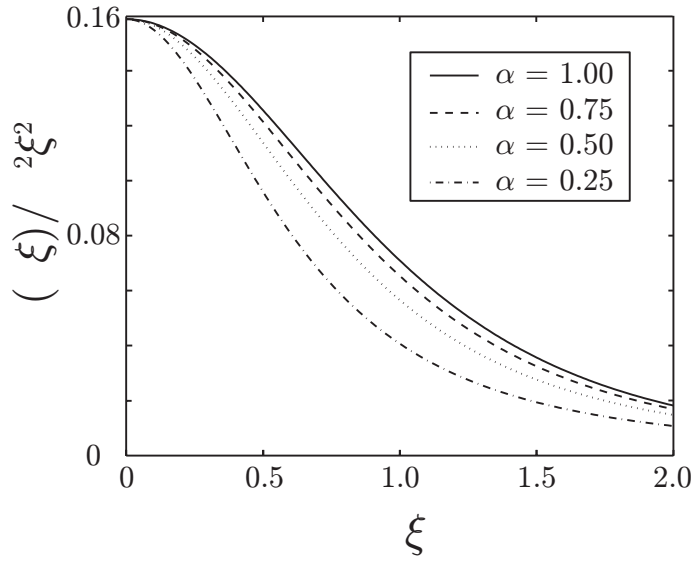

Fig. A.3. Sample self-affine PSD profiles from (A.68) for different values of α, including graphs with $\alpha = 1.00$, 0.75, 0.50, and 0.25.

Using the formula given by Watson [168],

$$\int_0^\infty K_\nu(x) x^{\mu-1} \mathrm{d}x = 2^{\mu-2}\Gamma\left(\frac{\mu-\nu}{2}\right)\Gamma\left(\frac{\mu+\nu}{2}\right),$$

the integral becomes

$$\begin{aligned} I &= \sum_{j=0}^{\infty} \frac{(-1)^j}{(j!)^2}\left(\frac{k}{2}\right)^{2j}\left[\left(\frac{\xi}{\sqrt{2\alpha}}\right)^{2j+\alpha+2} 2^{2j+\alpha}\Gamma\left(j+1\right)\Gamma\left(\alpha+j+1\right)\right] \\ &= \left(\frac{\xi}{\sqrt{2\alpha}}\right)^{\alpha+2} 2^{\alpha}\sum_{j=0}^{\infty}\frac{(-1)^j\Gamma\left(j+\alpha+1\right)}{j!}\left(\frac{k\xi}{\sqrt{2\alpha}}\right)^{2j} \\ &= \left(\frac{\xi}{\sqrt{2\alpha}}\right)^{\alpha+2} 2^{\alpha}\Gamma(\alpha+1)\sum_{j=0}^{\infty}\frac{\Gamma\left(j+\alpha+1\right)}{j!\Gamma(\alpha+1)}\left(-\frac{k^2\xi^2}{2\alpha}\right)^{j}. \end{aligned}$$

However, the series expansion for $(1+x^2)^{-\beta}$ is

$$\frac{1}{(1+x^2)^\beta} = \sum_{j=0}^{\infty}\frac{\Gamma(j+\beta)}{j!\Gamma(\beta)}\left(-x^2\right)^j,$$

which means the integral can be written as

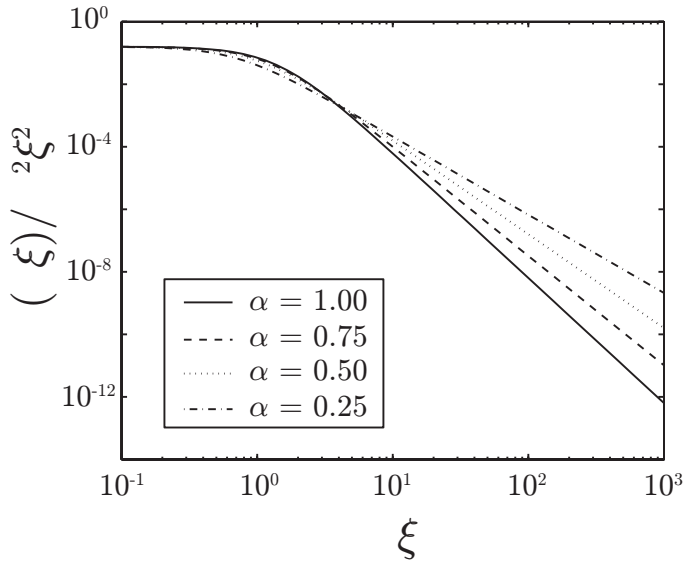

Fig. A.4. Sample self-affine PSD profiles on a log–log scale from (A.68) for different values of α, including graphs with $\alpha = 1.00$, 0.75, 0.50, and 0.25. The behavior of the PSD for large k is given by $P(k) \propto k^{-2-2\alpha}$.

$$I = \left(\frac{\xi}{\sqrt{2\alpha}}\right)^{\alpha+2} \frac{2^\alpha \Gamma(\alpha+1)}{\left(1+\frac{k^2\xi^2}{2\alpha}\right)^{1+\alpha}}.$$

Therefore, the Hankel transform of the autocorrelation function given in (A.63) is

$$\mathcal{H}\left\{\frac{\alpha}{2^{\alpha-1}\Gamma(\alpha+1)}\left(\frac{r}{\xi}\sqrt{2\alpha}\right)^\alpha K_\alpha\left(\frac{r}{\xi}\sqrt{2\alpha}\right)\right\} = \frac{\xi^2}{\left(1+\frac{k^2\xi^2}{2\alpha}\right)^{1+\alpha}}. \quad \text{(A.67)}$$

The PSD is $w^2/(2\pi)$ times the Hankel transform of the autocorrelation function from (2.22), which gives

$$P(k) = \frac{w^2\xi^2}{2\pi\left(1+\frac{k^2\xi^2}{2\alpha}\right)^{1+\alpha}}. \quad \text{(A.68)}$$

The full width at half maximum (FWHM) of this PSD is given by

$$\text{FWHM} = \frac{\sqrt{2\alpha(2^{1/(1+\alpha)}-1)}}{\xi}. \quad \text{(A.69)}$$

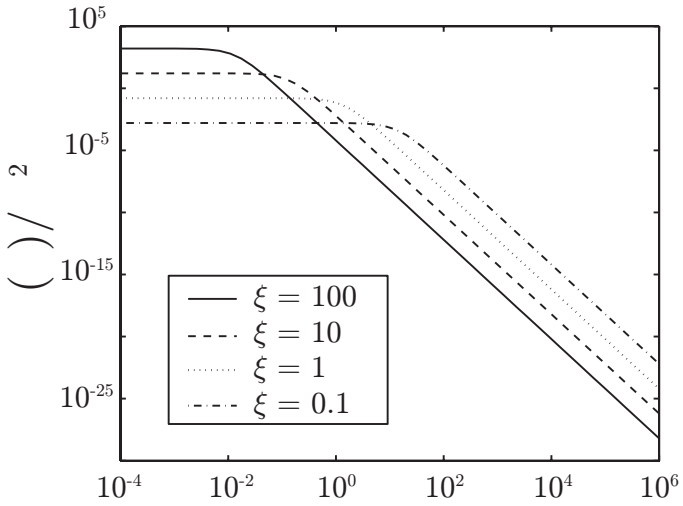

Fig. A.5. Sample self-affine PSD profiles on a log–log scale with different values for ξ from (A.68). Larger values of the correlation length ξ result in a smaller full width at half maximum (FWHM) as predicted by (A.69). All graphs have $\alpha = 1$.

For smaller values of the correlation length ξ, the PSD has a larger spread in frequency space, as seen in Fig. A.5. In addition, the behavior of the PSD for various values of α is shown in Fig. A.3, and on a log–log scale in Fig. A.4. The behavior of the PSD for large k is given by $P(k) \propto k^{-2-2\alpha}$, and thus the slope of the PSD on a log–log scale for large k will be equal to $-2 - 2\alpha$.

A.4.3 Mounded Surface – Exponential Model

The autocorrelation function for a mounded surface in 2+1 dimensions under the exponential model is

$$R(r) = \exp\left[-\left(\frac{r}{\xi}\right)^{2\alpha}\right] J_0\left(\frac{2\pi r}{\lambda}\right). \tag{A.70}$$

Because this autocorrelation function is the product of two functions, the PSD is proportional to the convolution of the two Hankel transforms from (A.53),

$$P(k) = \frac{w^2}{(2\pi)^2}\mathcal{H}\left\{\exp\left[-\left(\frac{r}{\xi}\right)^{2\alpha}\right]\right\} * \mathcal{H}\left\{J_0\left(\frac{2\pi r}{\lambda}\right)\right\}. \tag{A.71}$$

The Hankel transform of the Bessel function is given by (A.5),

$$\mathcal{H}\left\{J_0\left(\frac{2\pi r}{\lambda}\right)\right\} = \int_0^\infty r J_0\left(\frac{2\pi r}{\lambda}\right) J_0(kr)\mathrm{d}r = \frac{1}{k}\delta\left(k - \frac{2\pi}{\lambda}\right). \quad \text{(A.72)}$$

This relation is why the Bessel function is introduced in the autocorrelation function in (A.70) because the convolution integral in (A.71) is much simpler if one of the transforms is a delta function.

The Hankel transform of the exponential is more difficult, and we examine the case where $\alpha = 1$. The Hankel transform of the exponential when $\alpha = 1$ was found in Sect. A.4.1, and utilized in (A.60). The PSD is then given by the convolution of the two Hankel transforms. We must take care to take the convolution in Cartesian coordinates and then convert to polar to carry out the integral.

$$P(k) = \frac{w^2\xi^2}{8\pi^2}\int\int \exp\left[-\frac{\xi^2}{4}\left((k_x - x')^2 + (k_y - y')^2\right)\right] \times \frac{\delta\left(\sqrt{(x')^2 + (y')^2} - \frac{2\pi}{\lambda}\right)}{\sqrt{(x')^2 + (y')^2}}\mathrm{d}x'\mathrm{d}y'.$$

Changing variables from Cartesian coordinates (x', y') to polar coordinates (r, θ), $\mathrm{d}x'\mathrm{d}y' = r\mathrm{d}r\mathrm{d}\theta$, gives

$$P(k) = \frac{w^2\xi^2}{8\pi^2}\int_0^{2\pi}\int_0^\infty \exp\left[-\frac{\xi^2}{4}\left((k_x - r\cos\theta)^2 + (k_y - r\sin\theta)^2\right)\right] \times\delta\left(r - \frac{2\pi}{\lambda}\right)\mathrm{d}r\mathrm{d}\theta.$$

Integrating over the delta function,

$$P(k) = \frac{w^2\xi^2}{8\pi^2}\int_0^{2\pi} \exp\left[-\frac{\xi^2}{4}\left(\left(k_x - \frac{2\pi}{\lambda}\cos\theta\right)^2 + \left(k_y - \frac{2\pi}{\lambda}\sin\theta\right)^2\right)\right]\mathrm{d}\theta.$$

Expanding the argument of the exponential gives

$$P(k) = \frac{w^2\xi^2}{8\pi^2}\int_0^{2\pi} \exp\left[-\frac{\xi^2}{4}\left(k^2 + \frac{4\pi^2}{\lambda^2} - \frac{4\pi k_x}{\lambda}\cos\theta - \frac{4\pi k_y}{\lambda}\sin\theta\right)\right]\mathrm{d}\theta.$$

This can be simplified with the relation

$$a\cos\theta + b\sin\theta = \sqrt{a^2 + b^2}\cos\left(\theta - \tan^{-1}\frac{b}{a}\right),$$

which follows from the expansion of $\cos(x + y) = \cos x\cos y - \sin x\sin y$. Because the integral over θ is over a complete period of $\cos\theta$, the phase shift of $\tan^{-1} b/a$ does not affect the integral,

$$P(k) = \frac{w^2\xi^2}{8\pi^2}\int_0^{2\pi} \exp\left[-\frac{\xi^2}{4}\left(k^2 + \frac{4\pi^2}{\lambda^2} - \frac{4\pi k}{\lambda}\cos\theta\right)\right] \mathrm{d}\theta$$
$$= \frac{w^2\xi^2}{8\pi^2}\exp\left[-\frac{\xi^2}{4}\left(k^2 + \frac{4\pi^2}{\lambda^2}\right)\right]\int_0^{2\pi} \exp\left[\frac{\pi k\xi^2}{\lambda}\cos\theta\right] \mathrm{d}\theta.$$

From (A.11), this can be written as

$$P(k) = \frac{w^2\xi^2}{4\pi}\exp\left[-\frac{\left(4\pi^2 + k^2\lambda^2\right)\xi^2}{4\lambda^2}\right] I_0\left(\frac{\pi k\xi^2}{\lambda}\right). \tag{A.73}$$

This functional form assumes that $\alpha = 1$. For $\alpha \neq 1$, the Hankel transform of the exponential in the autocorrelation function can be expressed as a series from (A.58),

$$\mathcal{H}\left\{\exp\left[-\left(\frac{r}{\xi}\right)^{2\alpha}\right]\right\} = \frac{\xi^2}{2\alpha}\sum_{j=0}^{\infty}\frac{\Gamma\left(\frac{j+1}{\alpha}\right)}{(j!)^2}\left(-\frac{k^2\xi^2}{4}\right)^j. \tag{A.74}$$

There is clearly a problem when $\alpha = 0$, and this is addressed in the next section. Carrying out similar steps to the calculation with $\alpha = 1$, the PSD for general α can be expressed as a series,

$$P(k) = \frac{w^2\xi^2}{8\pi^2\alpha}\sum_{j=0}^{\infty}\frac{\Gamma\left(\frac{j+1}{\alpha}\right)}{(j!)^2}\left[-\frac{\pi k\xi^2}{a\lambda}\right]^j \int_0^{2\pi}[1 - a\cos\theta]^j \mathrm{d}\theta, \tag{A.75}$$

where $a = 4\pi\lambda k/\left(k^2\lambda^2 + 4\pi^2\right)$. This formula can be used for a numerical computation of the PSD for various values of α. We forgo further analysis of this form of the PSD because of the behavior for small α and introduce another autocorrelation function that is valid as $\alpha \to 0$.

A.4.4 Mounded Surface – *K*-Correlation Model

Consider the autocorrelation function

$$R(r) = \frac{\alpha}{2^{\alpha-1}\Gamma(\alpha+1)}\left(\frac{r}{\xi}\sqrt{2\alpha}\right)^{\alpha} K_\alpha\left(\frac{r}{\xi}\sqrt{2\alpha}\right) J_0\left(\frac{2\pi r}{\lambda}\right). \tag{A.76}$$

This is a combination of the autocorrelation function from the K-correlation model proposed for self-affine surfaces in Sect. A.4.2, along with the Bessel function introduced to model mounded surfaces. The advantage of this autocorrelation function is that we already know the Hankel transforms for both parts,

$$\mathcal{H}\left\{\frac{\alpha}{2^{\alpha-1}\Gamma(\alpha+1)}\left(\frac{r}{\xi}\sqrt{2\alpha}\right)^{\alpha} K_\alpha\left(\frac{r}{\xi}\sqrt{2\alpha}\right)\right\} = \frac{\xi^2}{\left(1 + \frac{k^2\xi^2}{2\alpha}\right)^{1+\alpha}}, \tag{A.77}$$

$$\mathcal{H}\left\{J_0\left(\frac{2\pi r}{\lambda}\right)\right\} = \frac{1}{k}\delta\left(k - \frac{2\pi}{\lambda}\right). \tag{A.78}$$

There are two reasons to consider this model for the autocorrelation function over the exponential model introduced in Sect. A.4.3. First, the exponential model for a mounded PSD diverges as $\alpha \to 0$, and the K-correlation model will remedy this behavior. Also, the functional form of the PSD for $\alpha = 1$ from the exponential model involves transcendental functions as given in (A.73), and is hard to analyze. We show that this new autocorrelation function gives a PSD that is a rational function for $\alpha = 1$. This allows us to analytically solve for the peak position k_m and see that it is equal to $2\pi\lambda^{-1}$ under certain conditions.

The Hankel transforms are already known, thus we can write the PSD as the convolution

$$P(k) = \frac{w^2}{4\pi^2} \int\int \frac{\xi^2}{\left[1 + \frac{\xi^2}{2\alpha}\left((k_x - x')^2 + (k_y - y')^2\right)\right]^{1+\alpha}} \times \frac{\delta\left(\sqrt{(x')^2 + (y')^2} - \frac{2\pi}{\lambda}\right)}{\sqrt{(x')^2 + (y')^2}} \mathrm{d}x'\mathrm{d}y'.$$

Transforming to polar coordinates gives

$$P(k) = \frac{w^2\xi^2}{4\pi^2} \int_0^{2\pi} \frac{\mathrm{d}\theta}{\left[1 + \frac{\xi^2}{2\alpha}\left(k^2 + \frac{4\pi^2}{\lambda^2} - \frac{4\pi k}{\lambda}\cos\theta\right)\right]^{1+\alpha}}.$$

It follows that the PSD is given by

$$P(k) = \frac{w^2\xi^2}{4\pi^2} \frac{1}{\left[1 + \frac{k^2\xi^2}{2\alpha} + \frac{2\pi^2\xi^2}{\alpha\lambda^2}\right]^{1+\alpha}} \int_0^{2\pi} \frac{\mathrm{d}\theta}{[1 - a\cos\theta]^{1+\alpha}}, \tag{A.79}$$

where

$$a = \frac{\frac{2\pi\xi^2 k}{\alpha\lambda}}{1 + \frac{k^2\xi^2}{2\alpha} + \frac{2\pi^2\xi^2}{\alpha\lambda^2}}.$$

This mounded PSD is pictured in Fig. A.6 for various values of α, and on a log–log scale in Fig. A.7. We first examine this equation with $\alpha = 1$, then discuss the expression for general α. For $\alpha = 1$, we need to use the result

$$\int_0^{2\pi} \frac{\mathrm{d}\theta}{(1 - a\cos\theta)^2} = \frac{2\pi}{(1 - a^2)^{3/2}}, \tag{A.80}$$

which can be found using complex variable techniques. The PSD becomes

$$P(k) = \frac{w^2\xi^2}{2\pi\left[1 + \frac{k^2\xi^2}{2} + \frac{2\pi^2\xi^2}{\lambda^2}\right]^2} \frac{1}{\left[1 - \left(\frac{\frac{2\pi\xi^2 k}{\lambda}}{1 + \frac{k^2\xi^2}{2} + \frac{2\pi^2\xi^2}{\lambda^2}}\right)^2\right]^{3/2}} \tag{A.81}$$

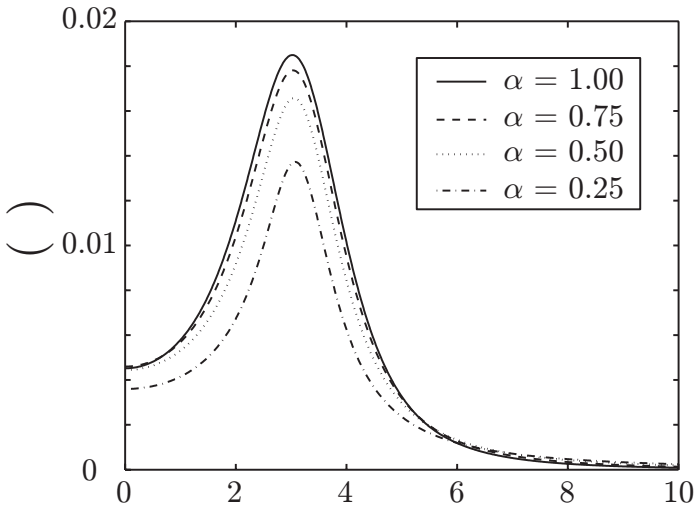

Fig. A.6. Sample mounded PSD profiles for different values of α from (A.79), including graphs with $\alpha = 1.00$, 0.75, 0.50, and 0.25. All graphs have $\lambda = 2$, $\xi = 1$, and $w = 1$. Note that the peak position lies at $k_m \approx \pi$, which corresponds to $2\pi/\lambda$.

$$= \frac{w^2\xi^2}{2\pi} \frac{1 + \frac{2\pi^2\xi^2}{\lambda^2} + \frac{\xi^2}{2}k^2}{\left[\left(1 + \frac{2\pi^2\xi^2}{\lambda^2} + \frac{\xi^2}{2}k^2\right)^2 - \left(\frac{2\pi\xi^2}{\lambda}k\right)^2\right]^{3/2}}. \tag{A.82}$$

This is the analytical form of the PSD for $\alpha = 1$, and it is expressed as a rational fraction. Now that we have an analytical PSD at our disposal, let us investigate the relation $k_m = 2\pi\lambda^{-1}$. To show this, we must set the derivative of the PSD with respect to k equal to zero and solve for k_m. Because the PSD is a rational function, the derivative will also be a rational function, and k_m can be obtained by setting the numerator of the derivative equal to zero. After some tedious algebra, one obtains

$$\lambda^4\xi^4k_m^4 + 4\lambda^2\xi^2(\pi^2\xi^2 + \lambda^2)k_m^2 - 4(2\pi^2\xi^2 + \lambda^2)(4\pi^2\xi^2 - \lambda^2) = 0.$$

This is a quadratic equation in k_m^2, with solution

$$k_m^2 = \frac{2\pi\xi\sqrt{4\lambda^2 + 9\pi^2\xi^2} - 2\pi^2\xi^2 - 2\lambda^2}{\lambda^2\xi^2}.$$

We are only concerned with positive wavenumbers, so k_m is given by

$$k_m = \frac{\sqrt{2\pi\xi\sqrt{4\lambda^2 + 9\pi^2\xi^2} - 2\pi^2\xi^2 - 2\lambda^2}}{\lambda\xi}.$$

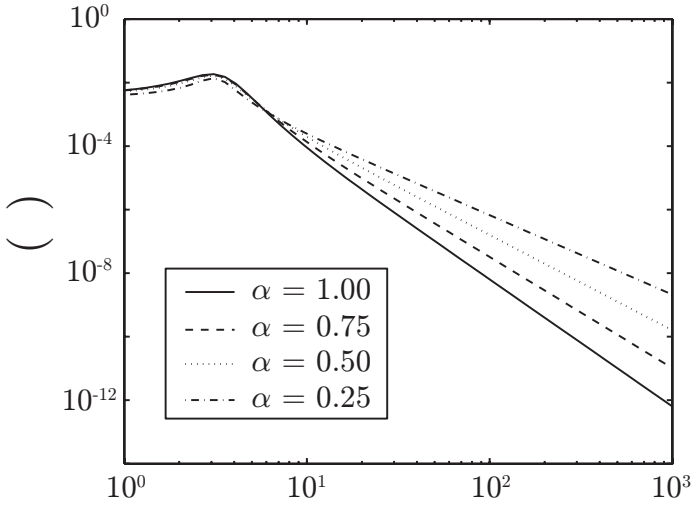

Fig. A.7. Sample mounded PSD profiles on a log–log scale for different values of α from (A.79), including graphs with $\alpha = 1.00$, 0.75, 0.50, and 0.25. All graphs have $\lambda = 2$, $\xi = 1$, and $w = 1$. The behavior of the PSD for large k is given by $P(k) \propto k^{-2-2\alpha}$.

This is certainly more complicated than the simple relation $k_m = 2\pi\lambda^{-1}$. However, with a rearrangement we obtain

$$k_m = \frac{\sqrt{6\pi^2\sqrt{1+\frac{4\lambda^2}{9\pi^2\xi^2}} - 2\pi^2 - \frac{2\lambda^2}{\xi^2}}}{\lambda}.$$

We can Taylor expand the innermost square root to obtain

$$k_m = \frac{\sqrt{4\pi^2 - \frac{2\lambda^2}{3\xi^2} + O\left(\frac{\lambda^4}{\xi^4}\right)}}{\lambda} = \frac{2\pi\sqrt{1 - \frac{\lambda^2}{6\pi^2\xi^2} + O\left(\frac{\lambda^4}{\xi^4}\right)}}{\lambda}.$$

Again Taylor expanding gives

$$k_m = \frac{2\pi}{\lambda}\left(1 - \frac{\lambda^2}{12\pi^2\xi^2} + O\left(\frac{\lambda^4}{\xi^4}\right)\right). \tag{A.83}$$

This gives us a condition when $k_m \approx 2\pi\lambda^{-1}$,

$$\frac{\lambda}{\xi} \ll 2\pi\sqrt{3} \approx 10.88. \tag{A.84}$$

Ordinarily, the wavelength is defined to be $\lambda \equiv 2\pi k_m^{-1}$, and the last result simply shows that (A.76) is consistent with this definition if the wavelength is not an order of magnitude larger than the correlation length. A different model for the autocorrelation function could give a better agreement with the relation $k_m = 2\pi\lambda^{-1}$, so there is room for improvement of this proposed model.

The full width at half maximum (FWHM) of this PSD is more complicated to determine, but in the regime where $\pi\xi\sqrt{2} \ll \lambda$, the PSD is a function of $k\xi$ only, which implies that FWHM $\propto \xi^{-1}$. Previous work has shown this behavior to be true through a numerical analysis [187]. It is a reasonable conclusion because the FWHM for a self-affine PSD is also inversely proportional to the lateral correlation length, as was shown in (A.69).

For a general value of α, expanding the integrand in (A.79) and using (A.43),

$$P(k) = \frac{w^2\xi^2}{2\pi\Gamma(\alpha+1)\left[1+\frac{k^2\xi^2}{2\alpha}+\frac{2\pi^2\xi^2}{\alpha\lambda^2}\right]^{1+\alpha}} \sum_{j=0}^{\infty} \frac{\Gamma(2j+\alpha+1)}{(j!)^2}\left(\frac{a^2}{4}\right)^j, \tag{A.85}$$

where

$$a = \frac{\frac{2\pi\xi^2 k}{\alpha\lambda}}{1+\frac{k^2\xi^2}{2\alpha}+\frac{2\pi^2\xi^2}{\alpha\lambda^2}}.$$

This form does not diverge as $\alpha \to 0$ as can be seen from an appropriate rearrangement of the PSD,

$$P(k) = \frac{w^2\xi^2(2\alpha)^{1+\alpha}}{2\pi\Gamma(\alpha+1)\left[2\alpha+k^2\xi^2+\frac{4\pi^2\xi^2}{\lambda^2}\right]^{1+\alpha}} \sum_{j=0}^{\infty} \frac{\Gamma(2j+\alpha+1)}{(j!)^2}\left(\frac{a^2}{4}\right)^j, \tag{A.86}$$

where

$$a = \frac{4\pi\xi^2\lambda k}{2\alpha\lambda^2+k^2\xi^2\lambda^2+4\pi^2\xi^2}.$$

However, recall from Sect. A.4.2 that the behavior of the PSD when $\alpha = 0$ must be treated separately in terms of the cutoff frequency k_c, which is not discussed here. A plot of this form of the PSD for various values of α is included in Fig. A.6. Changing the value of α does not significantly affect the peak position or the width of the peak, although smaller values of α yield a less pronounced peak intensity.

In the limit of large wavenumbers, $k \gg 2\pi/\lambda$, $a \approx 4\pi/(k\lambda)$, and the sum in (A.85) can be approximated by the first term. This gives

$$P(k \gg 2\pi/\lambda) \approx \frac{w^2\xi^2}{2\pi\left(1+\frac{k^2\xi^2}{2\alpha}\right)^{1+\alpha}}, \tag{A.87}$$

which is the form of a self-affine PSD from (A.68). This behavior is seen in Fig. A.7, which is graphed on a log–log scale. On a logarithmic scale, the slope of the graph for large k is $-2-2\alpha$. Therefore, at wavenumbers much larger than $2\pi/\lambda$, or equivalently at length scales much smaller than λ, the surface appears self-affine. Similarly, in the limit as $\lambda \to \infty$, $a \to 0$; and the PSD approaches the form of a self-affine PSD.

A.4.5 Summary

We present here a summary of the results for various forms of the power spectral density function in 1+1 and 2+1 dimensions. The mathematics of computing the PSD is similar in 1+1 dimensions to that presented in the previous sections for 2+1 dimensions. In 1+1 dimensions, the PSD can be expressed as

$$\begin{aligned} P(k) &= \frac{w^2}{2\pi}\int_{-\infty}^{\infty} R(r)\mathrm{e}^{-\mathrm{i}kr}\mathrm{d}r \\ &= \frac{w^2}{\pi}\int_{0}^{\infty} R(r)\cos kr\mathrm{d}r, \end{aligned}$$

where the integration over the imaginary part of the exponential drops out because the autocorrelation function $R(r)$ is even. By expanding $\cos kr$ in a Taylor series and integrating, the results for the PSD in 1+1 dimensions can be obtained. Because the mathematics is very similar to the derivations already presented, we simply summarize the results here. The only difference in the autocorrelation functions in 1+1 dimensions and 2+1 dimensions is the presence of a cos term in the mounded models instead of a Bessel function, which allows for the analytical expressions that follow.

1+1 Dimensions

- Self-affine exponential model:

$$R(r) = \exp\left[-\left(\frac{r}{\xi}\right)^{2\alpha}\right], \tag{A.88}$$

$$P(k) = \frac{w^2\xi}{2\pi\alpha}\sum_{j=0}^{\infty}\frac{\Gamma\left(\frac{j+1/2}{\alpha}\right)}{(2j)!}\left(-k^2\xi^2\right)^j. \tag{A.89}$$

- Self-affine exponential model ($\alpha = 1$):

$$R(r) = \exp\left[-\left(\frac{r}{\xi}\right)^{2}\right], \tag{A.90}$$

$$P(k) = \frac{w^2\xi}{2\sqrt{\pi}}\exp\left[-\frac{k^2\xi^2}{4}\right]. \tag{A.91}$$

- Self-affine K-correlation model:

$$R(r) = \frac{\alpha}{2^{\alpha-1}\Gamma(\alpha+1)} \left(\frac{r}{\xi}\sqrt{2\alpha}\right)^{\alpha} K_{\alpha}\left(\frac{r}{\xi}\sqrt{2\alpha}\right), \tag{A.92}$$

$$P(k) = \frac{w^2\xi}{\sqrt{2\pi}} \frac{\sqrt{\alpha}\Gamma(\alpha+1/2)}{\Gamma(\alpha+1)} \left(1+\frac{k^2\xi^2}{2\alpha}\right)^{-\alpha-1/2}. \tag{A.93}$$

- Mounded exponential model:

$$R(r) = \exp\left[-\left(\frac{r}{\xi}\right)^{2\alpha}\right] \cos\left(\frac{2\pi r}{\lambda}\right), \tag{A.94}$$

$$P(k) = \frac{w^2\xi}{4\pi\alpha} \sum_{j=0}^{\infty} \frac{\Gamma\left(\frac{j+1/2}{\alpha}\right)}{(2j)!} \left(-\xi^2\right)^j \left[\left(k-\frac{2\pi}{\lambda}\right)^{2j} + \left(k+\frac{2\pi}{\lambda}\right)^{2j}\right]. \tag{A.95}$$

- Mounded exponential model ($\alpha = 1$):

$$R(r) = \exp\left[-\left(\frac{r}{\xi}\right)^{2}\right] \cos\left(\frac{2\pi r}{\lambda}\right), \tag{A.96}$$

$$P(k) = \frac{w^2\xi}{2\sqrt{\pi}} \exp\left[-\frac{\left(4\pi^2+k^2\lambda^2\right)\xi^2}{4\lambda^2}\right] \cosh\left(\frac{\pi k\xi^2}{\lambda}\right). \tag{A.97}$$

- Mounded K-correlation model:

$$R(r) = \frac{\alpha}{2^{\alpha-1}\Gamma(\alpha+1)} \left(\frac{r}{\xi}\sqrt{2\alpha}\right)^{\alpha} K_{\alpha}\left(\frac{r}{\xi}\sqrt{2\alpha}\right) \cos\left(\frac{2\pi r}{\lambda}\right), \tag{A.98}$$

$$P(k) = \frac{w^2\xi}{2\sqrt{2\pi}} \frac{\sqrt{\alpha}\Gamma(\alpha+1/2)}{\Gamma(\alpha+1)} \left[\left(1+\frac{\left(k-\frac{2\pi}{\lambda}\right)^2\xi^2}{2\alpha}\right)^{-\alpha-1/2} + \left(1+\frac{\left(k+\frac{2\pi}{\lambda}\right)^2\xi^2}{2\alpha}\right)^{-\alpha-1/2}\right]. \tag{A.99}$$

2+1 Dimensions

- Self-affine exponential model:

$$R(r) = \exp\left[-\left(\frac{r}{\xi}\right)^{2\alpha}\right], \tag{A.100}$$

$$P(k) = \frac{w^2\xi^2}{4\pi\alpha}\sum_{j=0}^{\infty}\frac{\Gamma\left(\frac{j+1}{\alpha}\right)}{(j!)^2}\left(-\frac{k^2\xi^2}{4}\right)^j. \tag{A.101}$$

- Self-affine exponential model ($\alpha = 1$):

$$R(r) = \exp\left[-\left(\frac{r}{\xi}\right)^{2}\right], \tag{A.102}$$

$$P(k) = \frac{w^2\xi^2}{4\pi}\exp\left[-\frac{k^2\xi^2}{4}\right]. \tag{A.103}$$

- Self-affine K-correlation model:

$$R(r) = \frac{\alpha}{2^{\alpha-1}\Gamma(\alpha+1)}\left(\frac{r}{\xi}\sqrt{2\alpha}\right)^{\alpha}K_{\alpha}\left(\frac{r}{\xi}\sqrt{2\alpha}\right), \tag{A.104}$$

$$P(k) = \frac{w^2\xi^2}{2\pi\left(1+\frac{k^2\xi^2}{2\alpha}\right)^{1+\alpha}}. \tag{A.105}$$

- Mounded exponential model:

$$R(r) = \exp\left[-\left(\frac{r}{\xi}\right)^{2\alpha}\right]J_0\left(\frac{2\pi r}{\lambda}\right), \tag{A.106}$$

$$P(k) = \frac{w^2\xi^2}{8\pi^2\alpha}\sum_{j=0}^{\infty}\frac{\Gamma\left(\frac{j+1}{\alpha}\right)}{(j!)^2}\left[-\frac{\pi k\xi^2}{a\lambda}\right]^j\int_0^{2\pi}[1-a\cos\theta]^j\mathrm{d}\theta,$$

$$\text{where } a = \frac{4\pi\lambda k}{k^2\lambda^2+4\pi^2}. \tag{A.107}$$

- Mounded exponential model ($\alpha = 1$):

$$R(r) = \exp\left[-\left(\frac{r}{\xi}\right)^{2}\right]J_0\left(\frac{2\pi r}{\lambda}\right), \tag{A.108}$$

$$P(k) = \frac{w^2\xi^2}{4\pi}\exp\left[-\frac{\left(4\pi^2+k^2\lambda^2\right)\xi^2}{4\lambda^2}\right]I_0\left(\frac{\pi k\xi^2}{\lambda}\right). \tag{A.109}$$

- Mounded K-correlation model:

$$R(r) = \frac{\alpha}{2^{\alpha-1}\Gamma(\alpha+1)} \left(\frac{r}{\xi}\sqrt{2\alpha}\right)^{\alpha} K_{\alpha}\left(\frac{r}{\xi}\sqrt{2\alpha}\right) J_0\left(\frac{2\pi r}{\lambda}\right), \tag{A.110}$$

$$P(k) = \frac{w^2\xi^2}{2\pi\Gamma(\alpha+1)\left[1+\frac{k^2\xi^2}{2\alpha}+\frac{2\pi^2\xi^2}{\alpha\lambda^2}\right]^{1+\alpha}} \sum_{j=0}^{\infty} \frac{\Gamma(2j+\alpha+1)}{(j!)^2}\left(\frac{a^2}{4}\right)^j,$$

$$\text{where } a = \frac{4\pi\xi^2\lambda k}{2\alpha\lambda^2+k^2\xi^2\lambda^2+4\pi^2\xi^2}. \tag{A.111}$$

- Mounded K-correlation model ($\alpha = 1$):

$$R(r) = \frac{r\sqrt{2}}{\xi} K_1\left(\frac{r\sqrt{2}}{\xi}\right) J_0\left(\frac{2\pi r}{\lambda}\right), \tag{A.112}$$

$$P(k) = \frac{w^2\xi^2}{2\pi} \frac{1+\frac{2\pi^2\xi^2}{\lambda^2}+\frac{\xi^2}{2}k^2}{\left[\left(1+\frac{2\pi^2\xi^2}{\lambda^2}+\frac{\xi^2}{2}k^2\right)^2-\left(\frac{2\pi\xi^2}{\lambda}k\right)^2\right]^{3/2}}. \tag{A.113}$$

B

Euler's Method Implementation

The following is a C++ implementation of Euler's method to compute the solution to the partial differential equation

$$\frac{\partial h(x,t)}{\partial t} = \nabla^2 h(x,t) + \eta(x,t), \tag{B.1}$$

in one spatial dimension with cyclic boundary conditions and Gaussian distributed noise. A representative graph of the surface profile is included in Fig. B.1, and the evolution of the interface width is pictured in Fig. B.2.

```
#include <iostream>
#include <fstream>
#include <cmath>

using namespace std;

float* h;   //Stores h(x) at the current time
float* h_old;   //Stores h(x) at the previous time iteration
float delta_x = 1;
float delta_t = 0.001;
int N = 5000;  //Total length of domain = N*delta_x
int T = 10000;  //Total length of time = T*delta_t
float D = 1;  //Variance of the noise

float mean = 0;
float roughness = 0;

float laplacian(int j) //Computes the Laplacian of h(x)
{
      if(j == 0) //Cyclic boundary conditions
       return (h[j+1]-2*h[j]+h[N-1])/((delta_x)*(delta_x));
      else if(j == N-1) //Cyclic boundary conditions
```

```
         return (h[0]-2*h[j]+h[j-1])/((delta_x)*(delta_x));
        else
         return (h[j+1]-2*h[j]+h[j-1])/((delta_x)*(delta_x));
}

float noise()
{
      //Box-Muller transform to generate Gaussian random
      //variables with mean zero and variance one
      float x1, x2, k, y;

         do {
                 x1 = 2 * rand()/((float)RAND_MAX) - 1;
                 x2 = 2 * rand()/((float)RAND_MAX) - 1;
                 k = x1*x1 + x2*x2;
         } while ( k >= 1.0 );

         k = sqrt((-2.0*log(k))/k);
         y = x1 * k;

      return y;
}

int main()
{
   h = new float[N];
   h_old = new float[N];
   //Seed the random number generator
   srand((unsigned)time( NULL ));

   ofstream stats;
   stats.open("stats.txt");

   for(int i = 0; i < N; i++)
   {
        h[i] = 0;
   }

   for(int i = 0; i < N; i++)
   {
        h_old[i] = h[i];
   }

   //Iterate through time steps
   for(int k = 0; k < T; k++)
```

```
{

    //Iterate through position steps
    for(int j = 0; j < N; j++)
    {
    //Euler's Method
    h[j] = h_old[j]+
      delta_t*(laplacian(j)+sqrt( 2*D/
      ((delta_t)*(delta_x)*(delta_x)) )*noise());

    }

    //Iterate to next time step
    for(int i = 0; i < N; i++)
    {
           h_old[i] = h[i];
    }

    mean = 0;

    for(int i = 0; i < N; i++)
    {
           mean += h[i];
    }

    mean = mean / N;

    roughness = 0;

    for(int i = 0; i < N; i++)
    {
           roughness += (h[i]-mean)*(h[i]-mean);
    }

    roughness = sqrt(roughness / N);

    stats << k << " " << mean << " "
          << roughness << endl;

}

ofstream output;       //Output the results
output.open("result.txt");
 for(int i = 0; i < N; i++)
{
```

```
            output << i << " " << h[i] << endl;
        }

        return 0;

    }
```

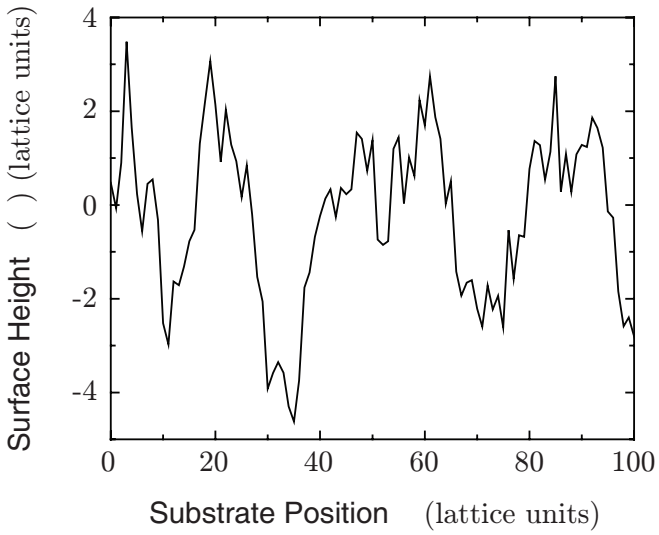

Fig. B.1. An example surface profile from the included code to model the Edwards–Wilkinson equation in one dimension. The position step size is $\Delta x = 1$, and the Gaussian noise has a variance $D = 1$.

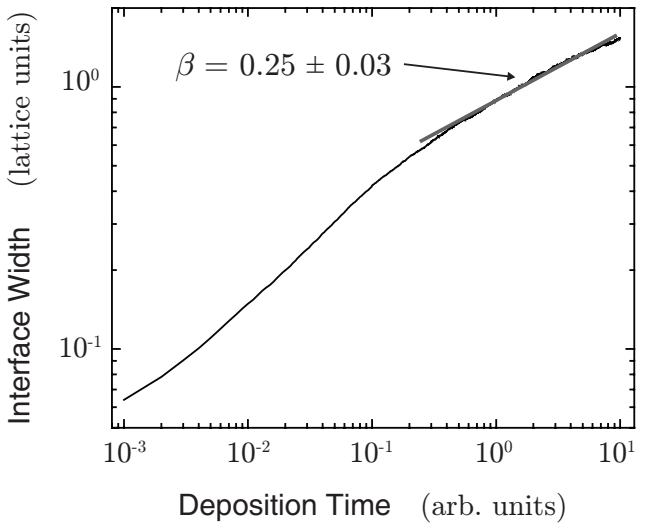

Fig. B.2. Interface width evolution of the Edwards–Wilkinson equation in one dimension calculated from the included code. The interface width evolves with an exponent $\beta = 0.25 \pm 0.03$, consistent with the discussion in Sect. 5.1.2 for $d = 1$.

C

Small World Model Implementation

The following is a C++ implementation of the small world model discussed in Chap. 6. This code simulates a small world network model with negative (shadowing) links between heights separated by a predetermined distance, $\lambda_0 = 10$ lattice units. This code can be modified to simulate surface growth under reemission and geometrical shadowing links as discussed in Chap. 6.

```
#include <iostream>
#include <cmath>
#include <fstream>
#include <time.h>
#include <string>

using namespace std;

const int N = 128;

float * Surface [N];
float * SurfaceNew [N];
float * links[N];

string filenm;
float D,deltat;
float deltax = 1;

float h(int x,int y)//Surface height
{
   while(x<0){x=x+N;}
   while(x>N-1){x=x-N;}

   while(y<0){y=y+N;}
   while(y>N-1){y=y-N;}
```

```
   return Surface[x][y];
}

float del2xy(int x, int y) //Laplacian
{
   return ( (h(x+1,y)+h(x-1,y)+
             h(x,y+1)+h(x,y-1)-
              (float)4*h(x,y) )/(deltax)*(deltax) );
}


float sw(int x, int y)
//Small world links for surface point at (x,y)
{
   float growth = 0;

    int shad_len = 10;
    //Shadowing length, or lambda_0
    //Heights are linked if separated by
    //a distance less than shad_len

    for(int k=-shad_len; k<=shad_len; k++)
    {
      for(int l=-shad_len; l<=shad_len; l++)
      {
           if( sqrt(k*k+l*l)<= shad_len)
            {
              growth +=  -(h(x+k,y+l)-h(x,y));
              //Link strength is negative
            }
      }
   }

   return growth;
}
float noise()
{
      //Box-Muller transform to generate Gaussian random
      //variables with mean zero and variance one
      float x1, x2, k, y;

         do {
                x1 = 2 * rand()/((float)RAND_MAX) - 1;
                x2 = 2 * rand()/((float)RAND_MAX) - 1;
```

```
                k = x1*x1 + x2*x2;
            } while ( k >= 1.0 );

            k = sqrt((-2.0*log(k))/k);
            y = x1 * k;

         return y;
}
void set_links() //Normalize link strength
{
     float sum = 0;
     float num = 0;

     for(int i = 0; i < N; i++)
     {
         for(int j = 0; j < N; j++)
         {
             num = sw(i,j);
             links[i][j]=num;
             //Find sum of link strengths
             sum += abs(num);
         }
     }

     if(sum == 0) return;

     //Normalize link strength
     for(int i = 0; i < N; i++)
     {
        for(int j = 0; j < N; j++)
        {
           links[i][j]=(links[i][j]/abs(sum))*N*N*25;
           //Choose strength of links to compete with
           //strength of random noise
        }
     }

     return;
}

float rms(float mean) //Surface roughness
{
   float roughness = 0;
   for(int i = 0; i < N; i++)
   {
```

```
         for(int j = 0; j < N; j++)
         {
            roughness += (h(i,j)-mean)*(h(i,j)-mean);
         }
      }
      return sqrt((double)roughness / (double)(N*N));
   }
   int main()
   {
      //Create Lattice
      filenm = "s1";
      deltat=0.025;
      D = 100;
      srand((unsigned)time(NULL));
      ofstream output2,output3;

      output2.open(string(filenm+string("_")
      +string("rms.txt")).c_str());

      output3.open("mean.txt");

      for (int i = 0;i < N;i++)
      {
         Surface [i] = new float [N];
         for(int j =0; j < N; j++)
         {
            Surface[i][j] = sqrt((float)(2*D)*
                    (deltat)/( (deltax)*(deltax)) )*noise();
         }
      }

      for (int i = 0;i < N;i++)
      {
         SurfaceNew [i] = new float [N];
         if(SurfaceNew[i]==0)
         {
            cerr << "Memory Error";
         }
      }

      for (int i = 0;i < N;i++)
      {
         links [i] = new float [N];
         if(links[i]==0)
         {
```

```
      cerr << "Memory Error";
   }
}

for(int t=1; t <= 500;t++)
{
   cout << "t = " << t <<endl;

   set_links();  //Normalize link strength
   for(int i = 0; i<N; i++)
   {
    for(int j = 0; j < N; j++)
    {
      SurfaceNew[i][j] = Surface[i][j]
      + deltat*(del2xy(i,j) + links[i][j]
      + sqrt( (float)(2*D)
        /((deltat)*(deltax)*(deltax)) )*noise());
    }
   }

   for(int i=0; i<N; i++)
   {
      for(int j = 0; j < N; j++)
      {
         Surface[i][j] = SurfaceNew[i][j];
      }
   }

   float mean = 0;
   for(int i=0; i<N; i++)
   {
      for(int j=0; j<N; j++)
      {
        mean += h(i,j);
      }
   }
   mean = mean / (float)(N*N);
   output3 << t << "\t" << mean << endl;

   float rough = rms(mean);
   output2 << t << "\t" << rough << endl;

   if(t%100 == 0) //Output surface profile
   {
      ofstream output;
```

```
            char fname[10];
            itoa(t,fname,10);
            output.open(string(filenm+string(" ")+
            string(fname)+string(".txt")).c_str());

            for(int i = 0; i < N; i++)
            {
               for(int j = 0; j < N; j++)
               {
                  output << h(i,j) << " ";
               }
               output << endl;
            }
            output.close();
         }
      }

      return 0;
   }
```

D

Solid-on-Solid Model Implementation

The following is a C++ implementation of the solid-on-solid model discussed in Sect. 8.1. This code models a deposition with normally incident particle flux and surface diffusion.

```
#include <iostream>
#include <fstream>
#include <string>
#include <cmath>

using namespace std;

const int N = 32768;
//Lattice size is N, must be less than or = (RAND_MAX - 1)
int h[N]; //Surface height array
double T = 1e8; // Number of particles to deposit

int jumps = 10; //Number of diffusion jumps

float mean = 0; //Mean surface height
float rough = 0; //Surface roughness

double Ea = 0.08; //Activation energy in eV
double kb = 8.6174e-5; //Boltzmann constant in eV/K
double Ts = 350; //Temperature of substrate in K
double En = 0.05; //Nearest neighbor activation energy

int height(int x)
//Returns surface height
{
    while(x < 0){ x += N;}
    while(x>(N-1)){ x -= N;}
```

```
    return h[x];
}

void deposit(int x)
//Increases surface height
{
    while(x < 0){ x += N;}
    while(x>(N-1)){ x -= N;}

    h[x]++;
}

void diffuse(int x, int xf)
//Diffuse particle from x to xf
{
    while(x < 0){ x += N;}
    while(x>(N-1)){ x -= N;}

    while(xf < 0){ xf += N;}
    while(xf>(N-1)){ xf -= N;}

    h[x]--;
    h[xf]++;
}

void evolve() //Add a new particle
{
     //Randomly choose initial deposition point
     //uniformly in [0,N-1]
     int x = -1;
     while (x<0 || x >(N-1)){ x = (int)( rand() );}

     deposit(x);

     //Particle diffusion
     for(int k = 0; k < jumps; k++)
     {
         //Choose particle to diffuse
         int l = -1;

          while (l<0 || l >(N-1)){ l = (int)( rand() );}
          int xd = l;
          if(height(xd)==0) continue;
          //Cannot diffuse if no particles
```

```
          int nn = 0; //Nearest neighbors
          //Count nearest neighbors
          for(int a = -1; a <=1; a++)
          {
               if(height(xd) <= height(xd+a)) nn++;
          }

         //Attempt to diffuse if particle has enough energy
         while((float)rand()/(RAND_MAX)
                < exp(-(Ea+nn*En)/(kb*Ts) ))
         {
             //Choose diffusion site
            int i = 0;
            while(i==0 || i < -1 || i > 1)
            {i = (int)( 2*((double)rand()/(RAND_MAX)
                        -0.5) * (2) );}

            //If diffusion site is no more
            //than 1 taller, diffuse
            int delta_h = (int) ( height(xd+i)-height(xd) );
            float delta_r = (float)
                             sqrt( delta_h*delta_h+ i*i );
            if (delta_h<=0 || delta_r<2 )
            {
                 diffuse(xd,xd+i);
                 xd = xd + i;
            }

            //Continue diffusing until Boltzmann factor
            //stops diffusion
            nn = 0;
            for(int a = -1; a <=1; a++)
            {
                 if(height(xd) <= height(xd+a)) nn++;
            }
         }
     }
}

int main()
{
    //Initialize random numbers
    srand( (unsigned)time( NULL ) );
```

```
ofstream output; //Output file streams
ofstream surface;
ofstream acf;

string filenm = "jump10";
//Filename for output files

output.open(string(filenm
                   +string("_stats.txt")).c_str());
surface.open(string(filenm
                    +string("_surface.txt")).c_str());

for(int i = 0; i < N; i++)
{
       h[i] = 0; //Flat initial surface
}

for(int t = 1; t <= T; t++)
{
      evolve(); //Add a new particle

      if(t%100000 == 0)
      {
         //Find mean height
         mean = 0;
         for(int i = 0; i < N; i++)
         {
            mean += h[i];
         }

         mean = (float) mean / (N);

         //Find roughness
         rough = 0;
         for(int i = 0; i < N; i++)
         {
            rough += (h[i] - mean)*(h[i] - mean);
         }

         rough = sqrt(rough / (N) );

         //Output mean height and roughness
         output << t << " " << mean << " "
                   << rough << endl;
```

```
            if(t%10000000 == 0)
            //Output autocorrelation function
            {
               char fname[15];
               itoa(t,fname,10);

               acf.open(string(filenm+string("_acf_")+
                string(fname)+string(".txt")).c_str());
               for(int dx = 0; dx < N/2; dx++)
               {
                  float sum = 0;
                  for(int i = 0; i < N; i++)
                  {
                     sum+= (height(i+dx)- mean)
                            *(height(i)-mean);
                  }

                    acf << dx<< " " << sum/(N) << endl;
               }
               acf.close();
            }

         }
    }

    for(int i = 0; i < N; i++) //Output surface profile
    {
           surface << i << " " <<(h[i] - mean)<<endl;
    }

   return 0;
}
```

References

1. J.G. Amar, F. Family, P.-M. Lam: Dynamic scaling of the island-size distribution and percolation in a model of submonolayer molecular-beam epitaxy. Phys. Rev. B **50**, 8781 (1994)
2. J.G. Amar, P.-M. Lam, F. Family: Groove instabilities in surface growth with diffusion. Phys. Rev. E **47**, 3242 (1993)
3. J.G. Amar, P.-M. Lam, F. Family: Surface growth with long-range correlated noise. Phys. Rev. A **43**, 4548 (1991)
4. G. Arfken, H. Weber: *Mathematical Methods for Physicists,* 5th edn (Harcourt Academic Press, New York 2001) p 711
5. P.B. Balbuena, J. M. Seminario: *Molecular Dynamics: From Classical to Quantum Methods* (Elsevier, New York 1999)
6. G.S. Bales, A.C. Redfield, A. Zangwill: Growth dynamics of chemical vapor deposition. Phys. Rev. Lett. **62**, 776 (1989)
7. G.S. Bales, A. Zangwill: Growth dynamics of sputter deposition. Phys. Rev. Lett. **63**, 692 (1989)
8. A.-L. Barabási, H.E. Stanley: *Fractal Concepts in Surface Growth* (Cambridge University Press, New York 1995)
9. A.-L. Barabási, H.E. Stanley: *Fractal Concepts in Surface Growth* (Cambridge University Press, New York 1995) p 19
10. A.-L. Barabási, H.E. Stanley: *Fractal Concepts in Surface Growth* (Cambridge University Press, New York 1995) p 27
11. A.-L. Barabási, H.E. Stanley: *Fractal Concepts in Surface Growth* (Cambridge University Press, New York 1995) p 213
12. A.-L. Barabási, H.E. Stanley: *Fractal Concepts in Surface Growth* (Cambridge University Press, New York 1995) p 289
13. D. Bensimon, B. Shraiman, S. Liang: On the ballistic model of aggregation. Physics Lett. A **102**, 238 (1984)
14. G.E.P. Box, M.E. Muller: A note on the generation of random normal deviates. Ann. Math. Stat. **29**, 610 (1958)
15. M. Boas: *Mathematical Methods in the Physical Sciences,* 2nd edn (John Wiley & Sons, New Jersey 1983) p 519
16. R. Bracewell: *The Fourier Transform and Its Applications,* 3rd edn (McGraw-Hill, New York 1999) pp 69–97

17. P. Brault, P. Dumas, F. Salvan: Roughness scaling of plasma-etched silicon surfaces. J. Phys.: Condens. Matter **10**, L27 (1998)
18. C. Buzea, G. Beydaghyan, C. Elliott, K. Robbie: Control of power law scaling in the growth of silicon nanocolumn pseudo-regular arrays deposited by glancing angle deposition. Nanotechnology **16**, 1986 (2005)
19. A.-C.-K. Chan, H. Wang, M.J. Chan: High quality thermal oxide on LPSOI formed by high temperature enhanced MILC. IEEE Electron Device Letters **22**, 384 (2001)
20. R. Chiarello, V. Panella, J. Krim, C. Thompson: X-ray reflectivity and adsorption isotherm study of fractal scaling in vapor-deposited films. Phys. Rev. Lett. **67**, 3408 (1991)
21. M. Constantin, C. Dasgupta, P.P. Chatraphorn, S.N. Majumdar, S. Das Sarma: Persistence in nonequilibrium surface growth. Phys. Rev. E **69** 061608 (2004)
22. Image courtesy of George T. Dalakos. G.T. Dalakos, J.P. Plawsky, P.D. Persans: Topographic evolution during deposition of plasma-deposited hydrogenated silicon on glass. Phys. Rev. B **72**, 205305 (2005)
23. S. Das Sarma, S.V. Ghaisas, J.M. Kim: Kinetic super-roughening and anomalous dynamic scaling in nonequilibrium growth models. Phys. Rev. E **49**, 122 (1994)
24. S. Das Sarma, C.J. Lanczycki, R. Kotlyar, S.V. Ghaisas: Scale invariance and dynamical correlations in growth models of molecular beam epitaxy. Phys. Rev. E **53**, 359 (1996)
25. S. Das Sarma, P. Tamborenea: A new universality class for kinetic growth: One-dimensional molecular-beam epitaxy. Phys. Rev. Lett. **66**, 325 (1991)
26. P. Dennery, A. Krzywicki: *Mathematics for Physicists* (Dover, New York 1995)
27. L. Devroye: *Non-Uniform Random Variate Generation* (Springer-Verlag, New York 1986)
28. C.V. Dharmadhikari, A.O. Ali, N. Suresh, D.M. Phase, S.M. Chaudhari, V. Ganesan, A. Gupta, B.A. Dasannacharya: Dynamic scaling in growth of platinum films on Si(100). Mater. Sci. Eng. B **75**, 29 (2000)
29. B. Dick, M.J. Brett, T. Smy, M. Belov, M.R. Freeman: Periodic submicrometer structures by sputtering. J. Vac. Sci. Technol. B **19**, 1813 (2001)
30. B. Dick, M.J. Brett, T.J. Smy, M.R. Freeman, M. Malac, R.F. Egerton: Periodic magnetic microstructures by glancing angle deposition. J. Vac. Sci. Technol. A **18**, 1838 (2000)
31. D. M. Dobkin, M. K. Zuraw, eds: *Principles of Chemical Vapor Deposition* (Springer, New York 2006)
32. Reprinted with permission from: J.T. Drotar, Y.-P. Zhao, T.-M. Lu, G.-C. Wang: Mechanisms for plasma and reactive ion etch-front roughening. Phys. Rev. B **61**, 3012 (2000); Copyright 2000 by the American Physical Society
33. J.T. Drotar, Y.-P. Zhao, T.-M. Lu, G.-C. Wang: Numerical analysis of the noisy Kuramoto-Sivashinsky equation in 2+1 dimensions. Phys. Rev. E **59**, 177 (1999)
34. J.T. Drotar, Y.-P. Zhao, T.-M. Lu, G.-C. Wang: Surface roughening in shadowing growth and etching in 2+1 dimensions. Phys. Rev. B **62**, 2118 (2000)
35. J.T. Drotar, Y.-P. Zhao, T.-M. Lu, G.-C. Wang: Surface roughening in low-pressure chemical vapor deposition. Phys. Rev. B **64**, 125411 (2001)
36. J.T. Drotar, Y.-P. Zhao, T.-M. Lu, G.-C. Wang: Why is KPZ type surface roughening so hard to observe?. Mat. Res. Soc. Proc. **648**, 7.9.1 (2001)

37. L. Dubost, A. Rhallabi, J. Perrin, J. Schmitt: Growth of nodular defects during film deposition. J. Appl. Phys. **78**, 3784 (1995)
38. S.F. Edwards, D.R. Wilkinson: The surface statistics of a granular aggregate. Proc. R. Soc. London Ser. A **381**, 17 (1982)
39. F. Family: Scaling of rough surfaces: Effects of surface diffusion. J. Phys. A: Math. Gen. **19**, L441 (1986)
40. F. Family, T. Vicsek: *Dynamics of Fractal Surfaces* (World Scientific Publishing Co., New Jersey 1991)
41. F. Family, T. Vicsek: Scaling of the active zone in the Eden process on percolation networks and the ballistic deposition model. J. Phys. A: Math. Gen. **18**, L75 (1985)
42. G. Fisherman: *Monte Carlo: Concepts, Algorithms, and Applications* (Springer-Verlag, New York 1995)
43. H. Guclu, G. Korniss: Extreme fluctuations in small-world networks with relaxational dynamics. Phys. Rev. E **69**, 065104 (2004)
44. K.H. Guenther: Microstructure of vapor-deposited optical coatings. Appl. Opt. **23**, 3806 (1984)
45. S. Hassani: *Mathematical Physics* (Springer-Verlag, New York 1999)
46. M.M. Hawkeye, M.J. Brett: Narrow bandpass optical filters fabricated with one-dimensionally periodic inhomogeneous thin films. J. Appl. Phys. **100**, 044322 (2006)
47. P.E. Hegeman, H.J.W. Zandvliet, G.A.M. Kip, A. van Silfhout: Kinetic roughening of vicinal Si(001). Surf. Sci. **311**, L655 (1994)
48. B M. Henry, Z. Xie, H. Smith, K.R. Kirov, V.M. Burlakov, C.R.M. Grovenor, H.E. Assender, G.A.D. Briggs, P.L. Burn, M. Kano, Y. Tsukahara: Characterization and performance of TiO-based solar cells. Proc. SPIE **5938**, 593817 (2005)
49. I. Hodgkinson, Q.H. Wu, S. Collett: Dispersion equations for vacuum-deposited tilted-columnar biaxial media. Appl. Opt. **40**, 452 (2001)
50. I. Hodgkinson, Q.H. Wu, J. Hazel: Empirical equations for the principal refractive indices and column angle of obliquely deposited films of tantalum oxide, titanium oxide, and zirconium oxide. Appl. Opt. **37**, 2653 (1998)
51. B. Holley, A. Faghri: Analysis of pulsating heat pipe with capillary wick and varying channel diameter. Int. J. of Heat and Mass Trans. **48**, 2635 (2005)
52. P. Hrudey, A. Popta, J. Sit, M. Brett: Photonic device applications of nanoengineered thin film materials. Proc. SPIE **5931**, 593113 (2005)
53. P. Jain, J.S. Juneja, T. Karabacak, E.J. Rymaszewski, T.-M. Lu: Surface roughness evolution in amorphous tantalum oxide films deposited by pulsed reactive sputtering. In: *Morphological and Compositional Evolution of Thin Films*, ed by M.J. Aziz, N.C. Bartelt, I. Berbezier, J.B. Hannon, S.J. Hearne. Mat. Res. Soc. Proc. **749**, W5.11 (2003)
54. J.H. Jeffries, J.-K. Zuo, M.M. Craig: Instability of kinetic roughening in sputter-deposition growth of Pt on glass. Phys. Rev. Lett. **76**, 4931 (1996)
55. M.D. Johnson, C. Orme, A.W. Hunt, D. Graff, J. Sudijono, L.M. Sander, B.G. Orr: Stable and unstable growth in molecular beam epitaxy. Phys. Rev. Lett. **72**, 116 (1994)
56. K. Kaminska, A. Amassian, L. Martinu, K. Robbie: Growth of vacuum evaporated ultraporous silicon studied with spectroscopic ellipsometry and scanning electron microscopy. J. Appl. Phys. **97**, 013511 (2005)

57. T. Karabacak, T.-M. Lu: Shadowing growth and physical self-assembly. In: *Handbook of Theoretical and Computational Nanotechnology,* ed by M. Rieth, W. Schommers (American Scientific Publishers, California 2005) ch 69
58. Reprinted with permission from: T. Karabacak, J.P. Singh, Y.-P. Zhao, G.-C. Wang, T.-M. Lu: Scaling during shadowing growth of isolated nanocolumns. Phys. Rev. B **68**, 125408 (2003); Copyright 2003 by the American Physical Society
59. Reprinted with permission from: T. Karabacak, Y.-P. Zhao, G.-C. Wang, T.-M. Lu: Growth-front roughening in amorphous silicon films by sputtering. Phys. Rev. B **64**, 085323 (2001); Copyright 2001 by the American Physical Society
60. T. Karabacak, Y.-P. Zhao, G.-C. Wang, T.-M. Lu: Growth front roughening in silicon nitride films by plasma-enhanced chemical vapor deposition. Phys. Rev. B **66**, 075329 (2002)
61. M. Kardar, G. Parisi, Y.C. Zhang: Dynamic scaling of growing interfaces. Phys. Rev. Lett. **56**, 889 (1986)
62. R.-P.-U. Karunasiri, R. Bruinsma, J. Rudnick: Thin-film growth and the shadow instability. Phys. Rev. Lett. **62**, 788 (1989)
63. E. Katzav: Self-consistent expansion for the molecular beam epitaxy equation. Phys. Rev. E **65**, 032103 (2002)
64. P. Keblinski, A. Maritan, F. Toigo, R. Messier, J.R. Banavar, Continuum model for the growth of interfaces. Phys. Rev. E **53**, 759 (1996)
65. S.R. Kennedy, M.J. Brett, H. Miguez, O. Toader, S. John: Optical properties of a three-dimensional silicon square spiral photonic crystal. Photonics and Nanostruct. Fundam. and Appl. **1**, 37 (2003)
66. S. Kennedy, M.J. Brett, O. Toader, S. John: Fabrication of tetragonal square spiral photonic crystals. Nano Lett. **2**, 59 (2001)
67. S.V. Kesapragada, D. Gall: Anisotropic broadening of Cu nanorods during glancing angle deposition. Appl. Phys. Lett. **89**, 203121 (2006)
68. J.M. Kim, S. Das Sarma: Discrete models for conserved growth equations. Phys. Rev. Lett. **72**, 2903 (1994)
69. S. Kim, N. Koratkar, T. Karabacak, T.-M. Lu: Water electrolysis activated by Ru nanorod array electrodes. Appl. Phys. Lett. **88**, 263106 (2006)
70. B. Kozma, M.B. Hastings, G. Korniss: Diffusion processes on power-law small-world networks. Phys. Rev. Lett. **95**, 018701 (2005)
71. B. Kozma, M.B. Hastings, G. Korniss: Roughness scaling for Edwards-Wilkinson relaxation in small-world networks. Phys. Rev. Lett. **92**, 108701 (2004)
72. J. Krug, P. Meakin: Columnar growth in oblique incidence ballistic deposition: Faceting, noise reduction, and mean-field theory. Phys. Rev. A **43**, 900 (1991)
73. Y. Kuo: *Thin Film Transistors: Materials and Processes* (Springer-Verlag, New York 2003).
74. Z.W. Lai, S. Das Sarma: Kinetic growth with surface relaxation: Continuum versus atomistic models. Phys. Rev. Lett. **66**, 2348 (1991)
75. A. Lakhtakia: Sculptured thin films: Accomplishments and emerging uses. Mater. Sci. Eng. C **19**, 427 (2002)
76. A. Lakhtakia, R. Messier: *Sculptured Thin Films: Nanoengineered Morphology and Optics,* (SPIE Press Monograph vol PM143, 2005).
77. C.-H. Lam, L.M. Sander: Surface growth with power-law noise. Phys. Rev. Lett. **69**, 3338 (1992)

78. P.-M. Lam, F. Family: Dynamics of a height-conserved surface-growth model with spatially correlated noise. Phys. Rev. A **44**, 7939 (1991)
79. Z. Lang, W. Xiuqin: Formation of nodular defects as revealed by simulation of a modified ballistic model of depositional growth. J. Mat. Sci. **33**, 1487 (1998)
80. H. Leschhorn, L.-H. Tang: Comment on 'Elastic string in a random potential'. Phys. Rev. Lett. **70**, 2973 (1993)
81. S. Liang, L.P. Kadanoff: Scaling in a ballistic aggregation model. Phys. Rev. A **31**, 2628 (1985)
82. C.-H. Lin, F. Yuan, C.-R. Shie, K.-F. Chen, B.-C. Hsu, M.H. Lee, W.W. Pai, C.W. Liu: Roughness-enhanced reliability of MOS tunneling diodes. IEEE Electron Device Letters **23**, 431 (2002)
83. A.V. Limaye, R.E. Amritkar: Theory of growth of ballistic aggregates. Phys. Rev. A **34**, 5085 (1986)
84. A. Lisfi, J.C. Lodder: Magnetic domains in Co thin films obliquely sputtered on a polymer substrate. Phys. Rev. B **63**, 174441 (2001)
85. F. Liu, M.T. Umlor, L. Shen, J. Weston, W. Eads, J.A. Barnard, G.J. Mankey: The growth of nanoscale structured iron films by glancing angle deposition. J. Appl. Phys. **85**, 5486 (1999)
86. G.P. Lepage: A new algorithm for adaptive multidimensional integration. J. Comp. Phys. **27**, 192 (1978)
87. J.M. López: Scaling approach to calculate critical exponents in anomalous surface roughening. Phys. Rev. Lett. **83**, 4594 (1999)
88. J.M. López, M.A. Rodríguez: Lack of self-affinity and anomalous roughening in growth processes. Phys. Rev. E **54**, R2189 (1996)
89. J.M. López, M.A. Rodríguez: Growth of interfaces with strong quenched disorder: Columnar media. Phys. Rev. E **52**, 6442 (1995)
90. J.M. López, M.A. Rodríguez, R. Cuerno: Superroughening versus intrinsic anomalous scaling of surfaces. Phys. Rev. E **56**, 3993 (1997)
91. T.-M. Lu, H.-N. Yang, G.-C. Wang: When interface gets rough.... Mat. Res. Soc. Symp. Proc. **367**, 283 (1995)
92. For review, see T.-M. Lu, Y.-P. Zhao, J.T. Drotar, T. Karabacak, G.-C. Wang: Novel mechanisms on the growth morphology of films. In: *Morphological and Compositional Evolution of Thin Films*, ed by M.J. Aziz, N.C. Bartelt, I. Berbezier, J.B. Hannon, S.J. Hearne. Mat. Res. Soc. Proc. **749**, W1.2 (2003)
93. D.R. Luhman, R.B. Hallock: Evidence for power-law dominated noise in vacuum deposited CaF_2. Phys. Rev. Lett. **92**, 256102 (2004)
94. M. Lutt, J.P. Schlomka, M. Tolan, J. Stettner, O.H. Seeck, W. Press: Kardar-Parisi-Zhang growth of amorphous silicon on Si/SiO_2. Phys. Rev. B **56**, 4085 (1997)
95. J. Mahan: *Physical Vapor Deposition of Thin Films* (John Wiley & Sons, Inc., New York 2000)
96. J. Mahan: *Physical Vapor Deposition of Thin Films* (John Wiley & Sons, Inc., New York 2000) p 29
97. J. Mahan: *Physical Vapor Deposition of Thin Films* (John Wiley & Sons, Inc., New York 2000) p 153
98. E. Main, T. Karabacak, T.-M. Lu: Continuum model for nanocolumn growth during oblique angle deposition. J. Appl. Phys. **95**, 4346 (2004)
99. S. Majaniemi, T. Ala-Nissila, J. Krug: Kinetic roughening of surfaces: Derivation, solution, and application of linear growth equations. Phys. Rev. B **53**, 8071 (1996)

100. B.B. Mandelbrot: Self-affine fractals and fractal dimension. Physica Scripta **32**, 257 (1985)
101. A. Margolina, H.E. Warriner: Growth in a restricted solid on solid model with correlated noise. J. Stat. Phys. **60**, 809 (1990)
102. J. Mathews, R. L. Walker: *Mathematical Methods of Physics,* 2nd edn (Addison-Wesley, New York 1970)
103. S.G. Mayr, K. Samwer: Tailoring the surface morphology of amorphous thin films by appropriately chosen deposition conditions. J. Appl. Phys. **91**, 2779 (2002)
104. P. Meakin: *Fractals, Scaling, and Growth Far from Equilibrium* (Cambridge University Press, New York 1998)
105. P. Meakin: *Fractals, Scaling, and Growth Far from Equilibrium* (Cambridge University Press, New York 1998) p 420
106. P. Meakin: *Fractals, Scaling, and Growth Far from Equilibrium* (Cambridge University Press, New York 1998) p 553
107. P. Meakin, J. Krug: Scaling structure in simple screening models for columnar growth. Phys. Rev. A **46**, 4654 (1992)
108. P. Meakin, R. Jullien: Restructuring effect in the rain model for random deposition. J. Physique **48**, 1651 (1987)
109. P. Meakin, R. Jullien: Spatially correlated ballistic deposition on one- and two-dimensional surfaces. Phys. Rev. A **41**, 983 (1990)
110. P. Meakin, R. Jullien: Spatially correlated ballistic deposition on one- and two-dimensional surfaces. Europhys. Lett. **9**, 71 (1989)
111. P. Meakin, P. Ramanlal, L.M. Sander, R.C. Ball: Ballistic deposition on surfaces. Phys. Rev. A **34**, 5091 (1986)
112. T. Michely, J. Krug: *Islands, Mounds, and Atoms: Patterns and Processes in Crystal Growth Far from Equilibrium* (Springer-Verlag, New York 2003)
113. D. Moldovan, L. Golubovic: Interfacial coarsening dynamics in epitaxial growth with slope selection. Phys. Rev. E **61**, 6190 (2000)
114. W.W. Mullins: Theory of thermal grooving. J. Appl. Phys. **28**, 333 (1957)
115. V. Ng, J.F. Hu, A.O. Adeyeye, J.P. Wang, T.C. Chong: Factors affecting surface roughness and coercivity of $Ni_{80}Fe_{20}$ thin films. J. Appl. Phys. **91**, 7206 (2002)
116. F. Ojeda, R. Cuerno, R. Salvarezza, L. Vázquez: Dynamics of rough interfaces in chemical vapor deposition: Experiments and a model for silica films. Phys. Rev. Lett. **84**, 3125 (2000)
117. S. Pal, D.P. Landau: Monte Carlo simulation and dynamic scaling of surfaces in MBE growth. Phys. Rev. B **49**, 10597 (1994)
118. G. Palasantzas: Roughness spectrum and surface width of self-affine fractal surfaces via the K-correlation model. Phys. Rev. B **48**, 14472 (1993)
119. G. Palasantzas: Self-affine fractals and the limit $H \to 0$. Phys. Rev. E **49**, 1740 (1994)
120. G. Palasantzas, J. Krim: Effect of the form of the height-height correlation function on diffuse x-ray scattering from a self-affine surface. Phys. Rev. B **48**, 2873 (1993)
121. A. Papoulis, *Probability, Random Variables, and Stochastic Processes,* 2nd edn (McGraw-Hill, New York 1984) pp 102–103
122. Reprinted with permission from: M. Pelliccione, T. Karabacak, C. Gaire, G.-C. Wang, T.-M. Lu: Mound formation in surface growth under shadowing. Phys. Rev. B **74**, 125420 (2006); Copyright 2006 by the American Physical Society

123. M. Pelliccione, T. Karabacak, T.-M. Lu: Breakdown of dynamic scaling in surface growth under shadowing. Phys. Rev. Lett. **96**, 146105 (2006)
124. Reprinted with permission from: M. Pelliccione, T.-M. Lu: Self-shadowing in ballistic fan formation from point seeds. Phys. Rev. B **75**, 245431 (2007); Copyright 2007 by the American Physical Society
125. C.-K. Peng, S. Havlin, M. Schwartz, H.E. Stanley: Directed polymer and ballistic-deposition growth with correlated noise. Phys. Rev. A **44**, R2239 (1991)
126. R. Pétri, P. Brault, O. Vatel, D. Henry, E. André, P. Dumas, F. Salvan: Silicon roughness induced by plasma etching, J. Appl. Phys. **75**, 7498 (1994)
127. J. Poortmans, V. Arkhipov, eds: *Thin Film Solar Cells: Fabrication, Characterization and Applications* (John Wiley & Sons, New York 2006)
128. F. Porcú, F. Prodi: Ballistic accretion on seeds of different sizes. Phys. Rev. A **44**, 8313 (1991)
129. W.H. Press, S.A. Teukolsky, W.T. Vetterling, B.P. Flannery, *Numerical Recipes: The Art of Scientific Computing,* 3rd edn (Cambridge University Press, New York 2007)
130. R. Rabady, I. Avrutsky: Reduced surface roughness of solid thin films prepared by alternating-bias, radio-frequency magnetron sputtering. J. Opt. Soc. Am. B **20**, 2174 (2003)
131. M. Raible, S.J. Linz, P. Hänggi: Amorphous thin film growth: Minimal deposition equation. Phys. Rev. E **62**, 1691 (2000)
132. P. Ramanlal, L.M. Sander: Theory of ballistic aggregation. Phys. Rev. Lett. **54**, 1828 (1985)
133. D.C. Rapaport: *The Art of Molecular Dynamics Simulation* (Cambridge University Press, New York 2004)
134. D. Reicher, P. Black, K. Jungling: Defect formation in hafnium dioxide thin films. Appl. Opt. **39**, 1589 (2000)
135. S.M. Rossnagel, T.S. Kuan: Alteration of Cu conductivity in the size effect regime. J. Vac. Sci. Technol. B **22**, 240 (2004)
136. P.I. Rovira, R.A. Yarussi, R.W. Collins, V.C. Venugopal, A. Lakhtakia, R. Messier, K. Robbie, M.J. Brett: Rotating-compensator multichannel transmission ellipsometry of a thin-film helicoidal bianisotropic medium. Thin Solid Films **313**, 373 (1998)
137. R.A. Roy, R.Messier: Preparation-physical structure relations in SiC sputtered films. J. Vac. Sci. Tech. A **2**, 312 (1984)
138. M. Saitou: Anomalous scaling of nickel surfaces in pulse-current electrodeposition growth. Phys. Rev. B **66**, 073416 (2002)
139. J. Shao, S. Wang, Z. Shen, X. Fu, H. He, Z. Fan: Glancing angle deposited thin films and their applications in laser systems. Proc. SPIE **6403**, 640312 (2006)
140. M. Siegert: Coarsening dynamics of crystalline thin films. Phys. Rev. Lett. **81**, 5481 (1998)
141. M. Siegert, M. Plischke: Slope selection and coarsening in molecular beam epitaxy. Phys. Rev. Lett. **73**, 1517 (1994)
142. S.K. Sinha, E.B. Sirota, S. Garoff, H.B. Stanley: X-ray and neutron scattering from rough surfaces. Phys. Rev. B **38**, 2297 (1988)
143. A.H.M. Smets, W.M.M. Kessels, M.C.M. van de Sanden: Temperature dependence of the surface roughness evolution during hydrogenated amorphous silicon film growth. Appl. Phys. Lett. **82**, 865 (2003)

144. D.L. Smith: *Thin Film Deposition: Principles and Practice* (McGraw-Hill, New York 1995) p 307
145. W.A. Smith: *Elementary Numerical Analysis* (Prentice Hall, New Jersey 1986) p 21
146. I.M. Sokolov, J. Mai, A. Blumen: Paradoxal diffusion in chemical space for nearest-neighbor walks over polymer chains. Phys. Rev. Lett. **79**, 857 (1997)
147. D. Sornette: *Critical Phenomena in Natural Sciences: Chaos, Fractals, Selforganization and Disorder: Concepts and Tools* (Springer, New York 2004) p 254
148. B.A. Sperling, J.R. Abelson: Kinetic roughening of amorphous silicon during hot-wire chemical vapor deposition at low temperature. J. Appl. Phys. **101**, 024915 (2007) and references therein
149. M.R. Spiegel, J. Liu: *Schaum's Outlines: Mathematical Handbook of Formulas and Tables,* 2nd edn (McGraw-Hill, New York 1999) p 109 eqn 18.71
150. H.E. Stanley: *Introduction to Phase Transition and Critical Phenomena* (Oxford University Press, New York 1971) p 108
151. C. Stolz, R. Tench, M. Kozlowski, A. Fornier: A comparison of nodular defect seed geometries from different deposition techniques. Proc. SPIE **2714**, 374 (1996)
152. J.A. Stroscio, D.T. Pierce, M.D. Stiles, A. Zangwill, L.M. Sander: Coarsening of unstable surface features during Fe(001) homoepitaxy. Phys. Rev. Lett. **75**, 4246 (1995)
153. S.M. Sze, K.K. Ng: *Physics of Semiconductor Devices,* 3rd edn (John Wiley & Sons, New York 2006)
154. D.M. Tanenbaum, A.L. Laracuente, A. Gallagher: Surface roughening during plasma-enhanced chemical-vapor deposition of hydrogenated amorphous silicon on crystal silicon substrates. Phys. Rev. B **56**, 4243 (1997)
155. C. Tang, S. Alexander, R. Bruinsma, B.E. Shaw: Scaling theory for the growth of amorphous films. Phys. Rev. Lett. **64**, 772 (1990)
156. F. Tang, T. Karabacak, L. Li, M. Pelliccione, G.-C. Wang, T.-M. Lu: Power-law scaling during shadowing growth of nanocolumns by oblique angle deposition. J. Vac. Sci. Tech. A **25**, 160 (2007)
157. F. Tang, D.-L. Liu, D.-X. Ye, Y.-P. Zhao, T.-M. Lu, A. Vijayaraghavan: Magnetic properties of Co nanocolumns fabricated by oblique-angle deposition. J. Appl. Phys. **93**, 4194 (2003)
158. R. Teki, N. Koratkar, T. Karabacak, T.-M. Lu: Enhanced photoemission from nanostructured surface topologies. Appl. Phys. Lett. **89**, 193116 (2006)
159. J.A. Thornton: High rate thick film growth. Annu. Rev. Mater. Sci. **7**, 239 (1977)
160. E.S. Tok, S.W. Ong, H.C. Kang: Dynamical scaling of sputter-roughened surfaces in 2+1 dimensions. Phys. Rev. E **70**, 011604 (2004)
161. F. Tsui, J. Wellman, C. Uher, R. Clarke: Morphology transition and layer-by-layer growth of Rh(111). Phys. Rev. Lett. **76**, 3164 (1996)
162. J.E. Van Nostrand, S.J. Chey, M.-A. Hasan, D.G. Cahill, J.E. Greene: Surface morphology during multilayer epitaxial growth of Ge(001). Phys. Rev. Lett. **74**, 1127 (1995)
163. J.A. Venables: *Introduction to Surface and Thin Film Processes* (Cambridge University Press, New York 2000) p 144
164. D. Vick, T. Smy, B. Dick, S. Kennedy, M.J. Brett: Growth behavior of engineered porous thin films - Measurement and modeling. Mat. Res. Soc. Symp. Proc. **648**, 3.43.1 (2001)

165. J. Villain: Continuum models of crystal growth from atomic beams with and without deposition. J. Phys. I (France) **1**, 19 (1991)
166. For review, see E.G. Wang: *Handbook of Theoretical and Computational Nanotechnology,* ed by M. Rieth, W. Schommers (American Scientific, California 2006) p 256
167. G.-C. Wang, T.-M. Lu: Physical realization of two-dimensional Ising critical phenomenon: Oxygen chemisorbed on a W(112) surface. Phys. Rev. **B** 31, 5918 (1985)
168. G.N. Watson: *A Treatise on the Theory of Bessel Functions* (Cambridge University Press, New York 1944) p 410
169. D.J. Watts: *Small Worlds: The Dynamics of Networks Between Order and Randomness* (Princeton University Press, New Jersey 1999)
170. D.J. Watts, S.H. Strogatz: Collective dynamics of 'small-world' networks. Nature (London) **393**, 440 (1998)
171. T.A. Witten Jr, L.M. Sander: Diffusion-limited aggregation, a kinetic critical phenomenon. Phys. Rev. Lett. **47**, 1400 (1981)
172. D.E. Wolf, J. Villain: Growth with surface diffusion. Europhys. Lett. **13**, 389 (1990)
173. J.-Q. Xi, J.K. Kim, E.F. Schubert, D. Ye, T.-M. Lu, S.-Y. Lin, J.S. Juneja: Very low-refractive-index optical thin films consisting of an array of SiO_2 nanorods. Opt. Lett. **31**, 601 (2006)
174. Reprinted with permission from: H.-N. Yang, Y.-P. Zhao, A. Chan, T.-M. Lu, G.-C. Wang: Sampling-induced hidden cycles in correlated random rough surfaces. Phys. Rev. B **56**, 4224 (1997); Copyright 1997 by the American Physical Society
175. H.-N. Yang, Y.-P. Zhao, G.-C. Wang, T.-M. Lu: Noise-induced roughening evolution of amorphous Si films grown by thermal evaporation. Phys. Rev. Lett. **76**, 3774 (1996)
176. A. Yanguas-Gil, J. Cotrino, A. Barranco, A.R. González-Elipe Influence of the angular distribution function of incident particles on the microstructure and anomalous scaling behavior of thin films. Phys. Rev. Lett. **96**, 236101 (2006)
177. J.H. Yao, H. Guo: Shadowing instability in three dimensions. Phys. Rev. E **47**, 1007 (1993)
178. J. Yao, C. Roland, H. Guo: Interfacial dynamics with long-range screening. Phys. Rev. A **45**, 3903 (1992)
179. D.-X. Ye, T.-M. Lu: Fanlike aggregations on seeds by parallel ballistic flux: Experimental results and Monte Carlo simulations of the growth of three-dimensional Si structures. Phys. Rev. B **75**, 115420 (2007)
180. D.-X. Ye, Z.-P. Yang, A.S.P. Chang, J. Bur, S.-Y. Lin, T.-M. Lu, R.Z. Wang, S. John: Experimental realization of a well-controlled 3D silicon spiral photonic crystal. J. Phys. D: Appl. Phys. **40**, 2624 (2007)
181. J. Yu, J.G. Amar: Dynamical scaling behavior in two-dimensional ballistic deposition with shadowing. Phys. Rev. E **66**, 021603 (2002)
182. Y.-C. Zhang: Growth anomaly and its implications. Physica A **170**, 1 (1990)
183. Y.-C. Zhang: Non-universal roughening of kinetic self-affine surfaces. J. Physique **51**, 2129 (1990)
184. Y.-P. Zhao, J.T. Drotar, G.-C. Wang, T.-M. Lu: Morphology transition during low-pressure chemical vapor deposition. Phys. Rev. Lett. **87**, 136102 (2001)
185. Y.-P. Zhao, J.T. Drotar, G.-C. Wang, T.-M. Lu: Roughening in plasma etch fronts of Si(100). Phys. Rev. Lett. **82**, 4882 (1999)

186. Y.-P. Zhao, J.B. Fortin, G. Bonvallet, G.-C. Wang, T.-M. Lu: Kinetic roughening in polymer film growth by vapor deposition. Phys. Rev. Lett. **85**, 3229 (2000)
187. Y.-P. Zhao, G.-C. Wang, T.-M. Lu: *Characterization of Amorphous and Crystalline Rough Surface: Principles and Applications* (Academic Press, New York 2001)
188. Y.-P. Zhao, D.-X. Ye, P.-I. Wang, G.-C. Wang, T.-M. Lu: Fabrication of Si nanocolumns and Si square spirals of self-assembled monolayer colloid substrates. Int. J. Nanosci. **1**, 87 (2002)
189. C.M. Zhou, D. Gall: Competitive growth of Ta nanopillars during glancing angle deposition: Effect of surface diffusion. J. Vac. Sci. Technol. A **25**, 312 (2007)
190. S. Zorba, Y. Shapir, Y. Gao: Fractal-mound growth of pentacene thin films. Phys. Rev. B **74** 245410 (2006)
191. J.-K. Zuo, J.F. Wendelken: Evolution of mound morphology in reversible homoepitaxy on Cu(100). Phys. Rev. Lett. **78**, 2791 (1997)

Symbols

ξ	Lateral Correlation Length
λ	Wavelength
w	Interface Width (Root-Mean-Square (RMS) Roughness)
$\overline{h}$	Mean Height
α	Roughness Exponent (Tilt of Surface Normal in Chap. 9)
β	Growth Exponent (Tilt of Columnar Growth in Chap. 9)
z	Dynamic Exponent (Aggregate Height in Chap. 9)
p	Wavelength Exponent (Aggregate Growth Exponent in Chap. 9)
$\eta(\mathbf{x}, t)$	Random Noise
$P(\mathbf{k}, t)$	Power Spectral Density Function (PSD)
$R(\mathbf{r}, t)$	Autocorrelation Function
$H(\mathbf{r}, t)$	Height–Height Correlation Function
k_m	Peak PSD Position
$J_n(x)$	nth Order Bessel Function of the First Kind
$I_0(x)$	Zeroth-Order Modified Bessel Function of the First Kind
$K_\alpha(x)$	α-order Modified Bessel Function of the Second Kind
$\delta(x)$	Delta Function
$\Gamma(x)$	Gamma Function
$\langle f(\mathbf{x}, t)\rangle$	Average Value of $f(\mathbf{x}, t)$
$\sim$	Similar Statistical Behavior
$\mathcal{F}$	Fourier Transform
$\mathcal{H}$	Hankel Transform
$\mathcal{P}$	Probability

Index

Springer Series in

MATERIALS SCIENCE

Editors: R. Hull R. M. Osgood, Jr. J. Parisi H. Warlimont

50 **High-Resolution Imaging and Spectrometry of Materials**
Editors: F. Ernst and M. Rühle

51 **Point Defects in Semiconductors and Insulators**
Determination of Atomic and Electronic Structure from Paramagnetic Hyperfine Interactions
By J.-M. Spaeth and H. Overhof

52 **Polymer Films with Embedded Metal Nanoparticles**
By A. Heilmann

53 **Nanocrystalline Ceramics**
Synthesis and Structure
By M. Winterer

54 **Electronic Structure and Magnetism of Complex Materials**
Editors: D.J. Singh and D. A. Papaconstantopoulos

55 **Quasicrystals**
An Introduction to Structure, Physical Properties and Applications
Editors: J.-B. Suck, M. Schreiber, and P. Häussler

56 **SiO_2 in Si Microdevices**
By M. Itsumi

57 **Radiation Effects in Advanced Semiconductor Materials and Devices**
By C. Claeys and E. Simoen

58 **Functional Thin Films and Functional Materials**
New Concepts and Technologies
Editor: D. Shi

59 **Dielectric Properties of Porous Media**
By S.O. Gladkov

60 **Organic Photovoltaics**
Concepts and Realization
Editors: C. Brabec, V. Dyakonov, J. Parisi and N. Sariciftci

61 **Fatigue in Ferroelectric Ceramics and Related Issues**
By D.C. Lupascu

62 **Epitaxy**
Physical Principles and Technical Implementation
By M.A. Herman, W. Richter, and H. Sitter

63 **Fundamentals of Ion-Irradiated Polymers**
By D. Fink

64 **Morphology Control of Materials and Nanoparticles**
Advanced Materials Processing and Characterization
Editors: Y. Waseda and A. Muramatsu

65 **Transport Processes in Ion-Irradiated Polymers**
By D. Fink

66 **Multiphased Ceramic Materials**
Processing and Potential
Editors: W.-H. Tuan and J.-K. Guo

67 **Nondestructive Materials Characterization**
With Applications to Aerospace Materials
Editors: N.G.H. Meyendorf, P.B. Nagy, and S.I. Rokhlin

68 **Diffraction Analysis of the Microstructure of Materials**
Editors: E.J. Mittemeijer and P. Scardi

69 **Chemical–Mechanical Planarization of Semiconductor Materials**
Editor: M.R. Oliver

70 **Applications of the Isotopic Effect in Solids**
By V.G. Plekhanov

71 **Dissipative Phenomena in Condensed Matter**
Some Applications
By S. Dattagupta and S. Puri

72 **Predictive Simulation of Semiconductor Processing**
Status and Challenges
Editors: J. Dabrowski and E.R. Weber

73 **SiC Power Materials**
Devices and Applications
Editor: Z.C. Feng

Springer Series in

MATERIALS SCIENCE

Editors: R. Hull R. M. Osgood, Jr. J. Parisi H. Warlimont

74 **Plastic Deformation in Nanocrystalline Materials**
By M.Yu. Gutkin and I.A. Ovid'ko

75 **Wafer Bonding**
Applications and Technology
Editors: M. Alexe and U. Gösele

76 **Spirally Anisotropic Composites**
By G.E. Freger, V.N. Kestelman, and D.G. Freger

77 **Impurities Confined in Quantum Structures**
By P.O. Holtz and Q.X. Zhao

78 **Macromolecular Nanostructured Materials**
Editors: N. Ueyama and A. Harada

79 **Magnetism and Structure in Functional Materials**
Editors: A. Planes, L. Mañosa, and A. Saxena

80 **Micro- and Macro-Properties of Solids**
Thermal, Mechanical and Dielectric Properties
By D.B. Sirdeshmukh, L. Sirdeshmukh, and K.G. Subhadra

81 **Metallopolymer Nanocomposites**
By A.D. Pomogailo and V.N. Kestelman

82 **Plastics for Corrosion Inhibition**
By V.A. Goldade, L.S. Pinchuk, A.V. Makarevich and V.N. Kestelman

83 **Spectroscopic Properties of Rare Earths in Optical Materials**
Editors: G. Liu and B. Jacquier

84 **Hartree–Fock–Slater Method for Materials Science**
The DV–X Alpha Method for Design and Characterization of Materials
Editors: H. Adachi, T. Mukoyama, and J. Kawai

85 **Lifetime Spectroscopy**
A Method of Defect Characterization in Silicon for Photovoltaic Applications
By S. Rein

86 **Wide-Gap Chalcopyrites**
Editors: S. Siebentritt and U. Rau

87 **Micro- and Nanostructured Glasses**
By D. Hülsenberg and A. Harnisch

88 **Introduction to Wave Scattering, Localization and Mesoscopic Phenomena**
By P. Sheng

89 **Magneto-Science**
Magnetic Field Effects on Materials: Fundamentals and Applications
Editors: M. Yamaguchi and Y. Tanimoto

90 **Internal Friction in Metallic Materials**
A Reference Book
By M.S. Blanter, I.S. Golovin, H. Neuhäuser, and H.-R. Sinning

91 **Time-dependent Mechanical Properties of Solid Bodies**
By W. Gräfe

92 **Solder Joint Technology**
Materials, Properties, and Reliability
By K.-N. Tu

93 **Materials for Tomorrow**
Theory, Experiments and Modelling
Editors: S. Gemming, M. Schreiber and J.-B. Suck

94 **Magnetic Nanostructures**
Editors: B. Aktas, L. Tagirov, and F. Mikailov

95 **Nanocrystals and Their Mesoscopic Organization**
By C.N.R. Rao, P.J. Thomas and G.U. Kulkarni

96 **Gallium Nitride Electronics**
By R. Quay

97 **Multifunctional Barriers for Flexible Structure**
Textile, Leather and Paper
Editors: S. Duquesne, C. Magniez, and G. Camino

98 **Physics of Negative Refraction and Negative Index Materials**
Optical and Electronic Aspects and Diversified Approaches
Editors: C.M. Krowne and Y. Zhang